Nature Communications

https://doi.org/10.1038/s41467-026-73071-7

Article in Press

Brain maintenance biomarkers from structural and functional interactions in aging and neurodegeneration

Received: 29 May 2025

Accepted: 28 April 2026

Cite this article as: Li, Y., Zhang, X., Li, X. *et al.* Brain maintenance biomarkers from structural and functional interactions in aging and neurodegeneration. *Nat Commun* (2026). https://doi.org/10.1038/s41467-026-73071-7

Yumeng Li, Xinyue Zhang, Xin Li & Zhanjun Zhang

Brain Maintenance Biomarkers from Structural and Functional Interactions in Aging and Neurodegeneration

Yumeng Li, B.D.[1,2,3], Xinyue Zhang, B.D.[1,2,3], Xin Li, Ph.D.[1,2,3*], Zhanjun Zhang, Ph.D.[1,2,3,4*]

[1] *State Key Laboratory of Cognitive Neuroscience and Learning, Beijing Normal University, Beijing, 100875, China*

[2] *Beijing Key Laboratory of Cognitive Intelligence for Elderly Brain Health, Beijing Normal University, Beijing, 100875, China*

[3] *Beijing Aging Brain Rejuvenation Initiative [1] Centre, Beijing Normal University, Beijing, 100875, China*

[4] *Innovation Institute of Integrated Traditional Chinese and Western Medicine, Shandong First Medical University & Shandong Academy of Medical Sciences, Jinan, Shandong, 250117, China*

*Correspondence to:

Xin Li, Ph.D., State Key Laboratory of Cognitive Neuroscience and Learning, Beijing Normal University, Beijing 100875, China;

Tel: +8601058802882;

Email addresses: lixin99@bnu.edu.cn

Zhanjun Zhang, Ph.D., State Key Laboratory of Cognitive Neuroscience and Learning, Beijing Normal University, Beijing 100875, China;

Tel: +8601058803882;

Email addresses: zhang_rzs@bnu.edu.cn

Abstract

Brain maintenance may help explain why some individuals remain cognitively resilient despite aging, but its biological basis is not well understood. Here we show that brain maintenance can be quantified from the relationship between brain structure and function. Using structural MRI and resting-state functional MRI from 1,280 older adults, we built a model based on young adults to estimate the functional capacity supported by preserved brain structure, and defined brain maintenance as the difference between predicted and observed function. Brain maintenance was most evident in prefrontal, cingulate and precuneus regions and was enriched in higher-order functional networks. Higher brain maintenance was associated with slower cognitive decline, lower amyloid-β burden and domain-specific variation in memory, attention and processing speed. These findings provide a biologically grounded marker of resilience in healthy and pathological aging.

Introduction

Brain maintenance (BM) refers to the relative preservation of brain integrity, encompassing stability in both structural and functional domains that account for variability in cognitive outcomes amid brain aging, pathology, or injury [2,3]. Its core lies in the resisting or slowing neural deterioration rather than deliberate activation. This maintenance model enables individuals to sustain cognitive performance by minimizing age- or disease-related brain changes. The relevant protective mechanisms may precede overt pathology. Also, Individual differences in brain maintenance reflect variability in the preservation of neural structure and function across aging [4,5].

Thus, accurately quantifying BM is vital for probing individual differences in late-life development and uncovering mechanisms underlying cognitive decline. Current BM quantification methods include: Longitudinal measures track within-person changes (e.g., annualized atrophy rates of hippocampal or cortical thickness), providing the most direct evidence of preservation but requiring costly multi-timepoint data and often subject to attrition [6,7]. Residual or cross-sectional measures, such as the brain age gap (Brain-PAD), compare an individual's brain to age-based normative expectations. While these approaches offer practical convenience without requiring longitudinal follow-up, they reflect deviation from population norms rather than within-person preservation over time. Therefore, they serve as indirect proxies of brain maintenance and may be influenced by model choice and cohort characteristics [8,9]. Functional or imaging-based metrics, including stability of network connectivity or region-specific atrophy rates, capture early, sensitive signs of aging and allow domain-specific insights, yet they are often noisier, modality-dependent, and may lack robust standardization [10,11] . Collectively, existing BM quantification strategies either demand longitudinal data, rely on indirect residual inferences, or suffer from variability in functional measures, underscoring the need for system-level indicators that integrate structure and function more directly.

Current evidence suggests that BM is most directly quantified by demonstrating reduced age-related change in brain structure over time, with functional neuroimaging

providing complementary, but not sufficient information. Sole reliance on either structural or functional metrics to index BM is limited, as the neural processes supporting maintenance operate at micro- and mesoscale levels that large-scale imaging can only approximate; integrating multimodal structure–function information therefore provides a more comprehensive estimate of the brain's preserved capacity [2,4,5]. While resting-state functional measures are task-independent and provide generalizable insights into large-scale brain dynamics, they cannot fully account for preserved brain integrity without considering the underlying structural architecture. Conversely, structural indices alone fail to capture the dynamic efficiency of functional systems that sustain cognition despite atrophy. Thus, structure and function must be viewed as interdependent contributors: only by integrating them can we comprehensively interpret the mechanisms of brain development and aging. Our research goal is therefore to establish a system-level framework for BM that bridges macro-level brain networks with micro-level neuronal mechanisms, offering a more precise and biologically grounded approach to quantifying maintenance.

Brain structure, particularly gray matter surface structure, is crucial for shaping neuronal signal transmission [12-15]. These structural features determine the physical characteristics of neural signal propagation, giving rise to complex patterns of neuronal co-activation. These highly ordered and dynamic activation patterns are considered key neural mechanisms supporting perception, cognition, and various psychological functions [16]. In the human brain, structural and functional decline in specific regions is not random but shows significant spatiotemporal synchrony [17,18]. That is, within similar time frames, the degradation of structural integrity and the reduction of functional efficiency in specific brain regions often occur together. Their interrelated evolution in particular brain areas jointly drives the overall trend of age-related cognitive changes, influencing cognitive performance and psychological states in old age.

The co-evolution of brain structure and function may indicate individual differences during aging. Within the BM framework, high-performing older adults often keep brain features similar to younger people. They show stronger structural integrity, more efficient neurotransmission, and more coherent connectivity [19,20]. This microscopic

neural infrastructure offers a stable resource base, helping individuals maintain cognitive function amid neurodegeneration or brain damage [4]. For instance, seniors with superior cognitive performance show high anatomical and physiological similarity to younger brains in structural integrity, neurotransmitter efficiency, and neural connectivity. Based on these features, cross-sectional studies can also help us understand individual differences in cognitive aging. Therefore, combining structural and functional measures may better capture BM differences and provide stronger clues to resilience in cognitive aging.

To address these gaps, this study proposes a framework for quantifying BM that leverages the interplay between brain structure and function. Our central premise is that the degree to which brain functional capacity can be maintained relative to underlying gray matter structure reflects an individual's capacity to maintain functional efficiency relative to structural integrity across aging. Specifically, our study design incorporated three complementary cohorts. First, a young adult reference group was used to establish an optimal structural–functional prediction model, providing a baseline of "youthful" brain organization. We selected individuals aged 18–20 years for the youthful reference model based on evidence that this age range corresponds to peak brain maturation and stable neuroanatomical profiles [17,21-23]. Second, a healthy older adult cohort from the Beijing Aging Brain Rejuvenation Initiative (BABRI) was included to represent normative aging, enabling assessment of interindividual differences in brain maintenance (BM) within a non-pathological population. Finally, a patient group with mild cognitive impairment [24] or Alzheimer's disease (AD) served as a pathological aging comparison, allowing us to test whether our metric could differentiate normal from abnormal aging trajectories. Together, these cohorts provided a coherent framework for investigating how brain structure–function correspondence can serve as an index of brain maintenance and its relationship to cognition and pathology in later life. The overall methodological framework, including data processing, BM quantification, and analytical modules, is illustrated in Figure 1.

Furthermore, recent research suggests that sex differences influence both the trajectory of brain aging and the neuroprotective effects of BM [25-29]. Therefore, our

study examines age- and sex-specific reconfigurations of structure–function maintenance networks to elucidate how these factors shape maintenance mechanisms during healthy and pathological aging.

The primary aims of this study are to: (1) identify spatially consistent BM networks—defined as brain networks that exhibit reproducible spatial patterns of BM across individuals, thereby providing insight into the neural substrates of maintenance mechanisms—that underpin cognitive resilience in aging, (2) characterize how these networks are reorganized with age and between sexes, [30] validate their ability to predict longitudinal cognitive decline and performance across different cognitive domains, and (4) determine whether these BM-driven network features can differentiate pathological aging (such as MCI/AD) from typical aging and predict amyloid-β deposition.

By integrating brain structural constraints with functional adaptability, our approach provides a biologically grounded, system-level BM metric that bridges macro- and micro-level mechanisms, offering insights into the heterogeneity of cognitive aging and guiding early intervention strategies.

Results

Participant Characteristics and Cognitive Function

The study sample comprised 1,280 healthy older adults (age range: 50–89 years; mean age: 66.45 ± 7.26 years; 61.4% female) for BM quantification. Within this cohort, 323 participants (baseline age: 50–86 years; mean: 65.74 ± 6.73 years; 61.3% female) underwent longitudinal cognitive assessments across 660 follow-up visits, with no significant demographic differences observed between this subgroup and the main cohort (independent t-tests, $p > 0.05$). The average follow-up duration was 3.19 ± 1.34 years. An independent validation cohort of 135 participants (mean age: 68.23 ± 8.09 years; 58.5% female), including cognitively normal (CN) individuals, mild cognitive impairment [24] patients, and Alzheimer's disease (AD) patients, was additionally analyzed. Detailed demographic characteristics and cognitive test performance metrics are summarized in Table 1.

Spatially Consistent Brain Maintenance Networks with Dominant High-Order

Functional Contributions

Using BM quantification methods outlined in the Statistical Analysis section, we mapped the whole-brain spatial distribution of BM values by averaging individual-level data across the aging cohort. As shown in Figure 2.a, BM exhibited pronounced spatial heterogeneity, characterized by a "anterior maintenance -posterior decline" pattern. Specifically, BM-rich regions clustered in the medial/lateral prefrontal cortex, superior temporal gyrus, pre-/postcentral gyri, cingulate cortex, and select parietal areas (e.g., precuneus). To assess the generalizability of this spatial pattern, we further constructed a population frequency map (Figure 2.b), representing the proportion of individuals (0–100%) in which each brain region was classified as a BM hub. Higher frequency values indicated greater spatial consistency of BM hubs across the population. Correlation analysis between regional BM values and hub frequency (Figure 2.c) revealed strong positive associations (cluster-level $p < 0.05$, FDR-corrected), confirming that BM-rich regions overlapped significantly with high-frequency hubs. By intersecting regions with above-average BM values (top 30%) and high hub frequency (>70%), we identified spatially consistent "core BM regions" in healthy older adults (Figure 2.d).

To delineate the functional architecture underlying these core regions, we parsed their composition across seven canonical functional networks (Figure 2.e). After normalizing for network size (i.e., parcel count), the Default Mode Network (DMN), Ventral Attention Network (VAN), and Frontoparietal Network (FPN) dominated BM hubs, collectively accounting for > 65% of all BM-rich regions. These networks are known for their high functional gradients and roles in integrative cognitive processes. Furthermore, ranking networks by total BM magnitude (summed BM values within each network) reaffirmed the prominence of DMN, VAN, and FPN (Figure 2.f), suggesting their critical involvement in sustaining cognitive resilience through adaptive functional mechanisms.

Age- and Sex-Stratified Differences in BM regions

We examined the impact of age, sex, and education on BM values within maintenance regions using covariate-adjusted residuals. Participants were stratified into younger-old (age ≤65 years) and older-old (age >65 years) groups. Age exerted

significant effects: younger-old adults exhibited higher BM values in the medial/lateral prefrontal cortex, middle frontal gyrus, and pre-/postcentral gyri, while older-old adults showed elevated BM in the fusiform gyrus, lingual gyrus, parahippocampal regions, and middle temporal gyrus (Figure 3.a). Sex differences were also pronounced: females demonstrated higher BM in the cingulate cortex, precuneus, superior frontal gyrus, and precentral gyrus, whereas males exhibited higher BM in the middle/superior frontal gyrus, superior temporal gyrus, fusiform gyrus, and parahippocampal regions (Figure 3.b). No significant BM differences were observed between high-education (≥14 years) and low-education groups. This result suggests that educational attainment alone may be insufficient to enhance dynamic neural adaptation measured by our BM metric. Potential explanations for this finding are further discussed in Discussion.

Further analysis of network-level BM differences revealed that younger-old adults displayed higher BM in the ventral attention (VAN), somatomotor (SomMot), frontoparietal network (FPN), and dorsal attention (DAN) networks but lower BM in visual (Vis) and limbic networks compared to older-old adults (Figure 3.c). Males exhibited higher BM in the default mode (DMN), FPN, and limbic networks, while females showed higher BM in SomMot and DAN networks (Figure 3.d). These findings underscore age- and sex-dependent reconfiguration of BM networks, with distinct functional domains preferentially contributing to cognitive resilience across demographic subgroups.

Domain-Specific and Cross-Phenotype Integration of BM regions Predict Cognitive performance

Using sparse canonical correlation analysis (SCCA), we identified four significant multivariate patterns linking BM spatial distributions to distinct cognitive phenotypes (processing speed, episodic memory, cognitive control, working memory). In the training dataset, these patterns exhibited significant associations (canonical r = 0.15–0.23, Bonferroni-corrected $p < 0.05$), which were replicated in the test dataset (r = 0.10–0.20, Bonferroni-corrected $p < 0.05$). To further validate statistical significance, we performed permutation testing with 10,000 random shuffles of the data. The observed canonical correlations in the test dataset were significantly greater than chance (all

permutation $p < 0.05$ after Bonferroni correction), supporting the robustness of the identified brain–cognition relationships. Figure 4.b shows the contribution weights of neuropsychological tests in the four cognitive phenotypes. Each phenotype mapped to spatially distinct BM hubs (Figure 4.a). For instance, the maintenance regions for processing speed phenotypes are mainly in the right supramarginal gyrus, middle cingulate gyrus, and left precuneus. For episodic memory phenotypes, they are focused in the bilateral superior frontal gyrus, left middle cingulate gyrus, and medial superior frontal gyrus. Cognitive control related regions lie in the inferior orbital frontal and anterior cingulate regions, and those for working memory phenotypes are related in the right middle temporal gyrus and precuneus.

Notably, the postcentral gyrus and superior frontal gyrus contributed to all four phenotypes, while the middle cingulate and precuneus supported multiple phenotypes (Figure 4.b), suggesting that BM hubs form flexible subsystems through combinatorial arrangements to support diverse cognitive demands.

Furthermore, the summed BM values of phenotype-specific hubs strongly correlated with composite cognitive scores (weighted by neuropsychological test contributions). This relationship was most pronounced for episodic memory and working memory (Figure 4.c), indicating that higher BM in targeted networks predicts superior domain-specific performance.

BM Networks Predict Multi-Domain Attenuation of Cognitive Decline in Aging

To validate whether elevated BM values in maintenance regions correlate not only with better baseline cognitive performance but also with slower longitudinal cognitive decline, we calculated annualized cognitive decline rates (see Methods) and examined their associations with regional BM values. Spatial mapping revealed distinct BM hubs significantly linked to reduced decline rates across cognitive domains (Figure 5.a & c). The most extensive BM-protective effects were observed for general cognition (MMSE) and working memory (DST), followed by visuospatial (CDT) and language (VFT) domains. In contrast, episodic memory (AVLT), processing speed (TMT-A), and cognitive control (SCWT) exhibited narrower, phenotype-specific BM associations.

Aggregating BM values across decline-related hubs demonstrated a statistically

significant but modest correlation between total BM and global cognitive alternation rates (Figure 5.b & d), indicating that higher BM predicts slower aging-related cognitive deterioration. These findings position BM as a quantifiable neuroprotective biomarker, aligning with theoretical frameworks of brain maintenance that emphasize adaptive resilience against age- and pathology-driven functional decline.

BM value Reveal Disease Stage-Specific Vulnerability

Comparative analysis of BM distributions across cognitively normal (CN), mild cognitive impairment [24], and Alzheimer's disease (AD) groups revealed distinct neurobiological signatures of pathological aging. While spatial BM patterns in CN and pathological groups (MCI/AD) showed no global differences (Figure 6.a), summed BM values across maintenance regions were significantly higher in CN compared to MCI and AD (Figure 6.b), with no MCI-AD group differences. Network-level analyses of covariate-adjusted BM residuals demonstrated that MCI exhibited pronounced BM reductions in the default mode (DMN), ventral attention (VAN), frontoparietal (FPN), and limbic networks relative to CN, whereas AD showed BM deficits only in VAN (Figures 6.c).

Spatial mapping of group differences (Figures 7.d) highlighted broader BM reductions in MCI compared to AD, particularly in anterior medial/lateral prefrontal and temporal regions—key hubs of brain maintenance (Figures 6.e). Notably, BM differences in overlapping regions (e.g., superior frontal gyrus) were minimal between MCI and AD, suggesting MCI-specific vulnerability preceding widespread AD pathology. Furthermore, BM deficits in MCI/AD significantly correlated with domain-specific cognitive decline (e.g., memory, executive function; Figure 6.f), reinforcing BM's role as a mediator of clinical symptom severity.

These findings identify MCI as a critical window of BM network sensitivity, offering early biomarkers for pathological progression, while underscoring the divergent neuroadaptive trajectories between MCI and AD.

BM Networks Predict Stage-Specific Aβ Deposition

Using a leave-one-out cross-validated generalized linear regression framework (see Methods), we evaluated the ability of BM values in maintenance regions to predict

whole-brain Aβ deposition across cognitively normal (CN), mild cognitive impairment [24], and Alzheimer's disease (AD) groups. In the All group (CN+MCI+AD) and CN group, BM hubs exhibited limited predictive sensitivity, with only the inferior orbital frontal cortex showing modest associations (Figure 7.a). In AD, predictive efficacy extended to the Rolandic operculum and precentral gyrus, while MCI demonstrated the highest sensitivity, with BM hubs in the superior/middle temporal gyri, middle cingulate, precuneus, and Heschl's gyrus predicting Aβ deposition.

Critically, aggregated BM values from top-predictive hubs inversely correlated with global Aβ burden (Figure 7.b), indicating that higher BM is associated with reduced amyloid pathology. This relationship was strongest in MCI, suggesting BM networks act as early neuroprotective buffers against amyloid accumulation during the preclinical phase. Statistical analyses in Figure 7 were performed using BM values extracted from predictive hubs identified by cross-validation, calculated across all subjects in each group.

Discussion

This study established a metric for quantifying brain maintenance (BM), integrating brain functional signatures that best capture BM characteristics with structural underpinnings to elucidate its neurobiological mechanisms. The spatial distribution of BM values across a large aging cohort revealed core maintenance hubs concentrated in the prefrontal cortex, cingulate gyrus, and precuneus, predominantly organized within high-order functional networks—including the default mode network (DMN), ventral attention network (VAN), and frontoparietal network (FPN). Domain-specific cognitive phenotypes (processing speed, episodic memory, cognitive control, working memory) exhibited distinct spatial associations with BM networks, where key regions (e.g., postcentral gyrus, superior frontal gyrus, middle cingulate) formed domain-linked subsystems to support cognition through combinatorial interactions. These associations are correlational, and while they may reflect adaptive processes, they should not be interpreted as direct evidence of compensation. Longitudinal analyses demonstrated significant negative correlations between BM values and rates of cognitive decline,

indicating that elevated BM predicts attenuated aging-related cognitive deterioration. Pathological aging cohorts (MCI and AD) showed markedly reduced BM compared to cognitively normal (CN) individuals, with MCI exhibiting greater sensitivity to BM alterations than AD, particularly in prefrontal and temporal hubs. Critically, BM deficits were robustly associated with increased Aβ deposition, highlighting its potential as an early biomarker for preclinical amyloid pathology. These findings position BM as a multifaceted neuroprotective framework, bridging functional resilience, structural integrity, and pathological progression, while offering actionable targets for interventions aimed at mitigating cognitive decline in aging and neurodegeneration.

While these results indicated structure–function–cognition associations, it is important to contextualize their interpretation. Resting-state FC is inherently more domain-general than task-evoked activation; however, a large body of evidence demonstrates that intrinsic connectivity nonetheless exhibits systematic links to specific cognitive domains. For instance, prefrontal–parietal hubs are consistently associated with executive function, and DMN connectivity with episodic memory [31-33]. This literature supports the plausibility of the domain-specific associations observed here, even in the absence of task-related activity. At the same time, not all associations conform neatly to expectations. The involvement of the postcentral gyrus—a primary somatosensory region—in higher-order cognitive associations is somewhat unexpected, as age-related connectivity changes are typically most pronounced in higher-order networks while primary sensorimotor networks show more variable effects [34]. One possible interpretation is that, in older adults, the postcentral gyrus increases its integrative coupling with higher-order networks as sensory integrity declines, reflecting functional upregulation or rerouting [35,36].

The pronounced heterogeneity in cognitive aging presents a critical challenge for unraveling its mechanisms and mitigating aging-related decline. BM serves as a pivotal concept in elucidating this phenomenon [37]. From a lifespan developmental perspective, individual differences in cognitive aging manifest primarily in two dimensions: the peak cognitive performance achieved in early adulthood and the subsequent rate of decline with advancing age [38,39]. However, contemporary research highlights the role

of adaptive strategies employed during aging. It is posited that BM refers to preserved neural integrity across aging, which may be associated with reduced accumulation or expression of age-related pathology [40]. Prior studies demonstrate that BM modifies the relationship between brain structure and cognition: individuals with higher BM exhibit superior cognitive performance despite comparable gray matter volume or white matter integrity, suggesting more efficient utilization of available neural resources [41-43]. Furthermore, elevated BM is associated with preserved brain network efficiency even amid gray matter atrophy [44,45]. Our BM metric advances prior frameworks by directly quantifying neurobiological reserve, capturing older adults' capacity to flexibly adapt to developmental changes. Strikingly, we identified "maintenance hubs"—brain regions where functional activity in older adults exceeds the maximal threshold predicted by youthful structural models. These hubs exhibit high inter-individual spatial consistency, yet the magnitude of functional excess varies systematically, reflecting individual differences in BM. This divergence underscores BM's role in buffering age-related neural decline while highlighting its potential as a biomarker for personalized cognitive resilience strategies.

Notably, the identified BM hubs—localized to the medial/lateral frontal cortex [46-48], cingulate cortex [49,50], and precuneus [51,52] — reflect intrinsic neurobiological mechanisms underlying brain maintenance. The BM regions, predominantly organized within high-order functional networks (default mode network [DMN], ventral attention network [VAN], and frontoparietal network [FPN]), occupy apex positions along functional gradients and serve as integrative hubs for cross-modal information processing [53]. Longitudinal studies of cortical atrophy reveal divergent trajectories between normal and pathological aging: typical aging exhibits relatively uniform atrophy across frontal and temporal regions, whereas pathological aging (e.g., Alzheimer's disease [AD]) is characterized by accelerated atrophy focused in the temporal lobe, with relative sparing of prefrontal regions [54]. Further analyses of low-risk populations (Aβ-negative, APOE ε4 non-carriers) demonstrate that mild cognitive impairment [24] and AD cohorts exhibit maximal standardized atrophy rates in temporal regions, while low-risk individuals retain a frontal-temporal balanced atrophy pattern

resembling normal aging [55,56]. According to the multiple factor framework of brain aging [57,58], pathological cognitive aging (PCA) and normal cognitive aging [59] follow distinct trajectories: PCA is driven by early medial temporal lobe vulnerability and rapid pathological spread, whereas NCA predominantly involves gradual decline in fronto-striatal circuitry. Critically, our BM hubs overlap extensively with fronto-striatal networks, suggesting that BM variations in these hubs are critical markers of individual differences in developmental trajectories among the NCA cohort [60]. Individuals failing to achieve NCA-level BM in these hubs may face elevated risks of transitioning to PCA, highlighting BM's dual role as both a biomarker of resilience and a predictor of pathological progression.

Brain maintenance, as a neurobiological property of the brain, reflects the preservation of neural structure and function that minimizes age-related neural decline, thereby supporting stable cognitive performance. Neuroplasticity—the brain's ability to optimize neural circuit efficiency and adapt to internal and external demands—provides a physiological foundation for BM [61]. In the context of memory aging, neuroplastic mechanisms operate through three primary pathways: neurogenesis (generation of new neurons), structural remodeling (strengthened connectivity, volumetric expansion, or reorganization of existing pathways), and functional engagement (adaptive reconfiguration of activation patterns) [62]. While neurogenesis and structural remodeling are resource-intensive and decline with aging, functional engagement emerges as a dominant adaptive strategy. The functional plasticity hypothesis of cognitive aging posits that structural atrophy impairs region-specific processes, yet the aging brain compensates by recruiting alternative regions (e.g., prefrontal and parietal cortices) to support task performance [63-65]. Our findings extend this framework by illustrating functional reorganization consistent with previously described forms of age-related plasticity: older adults in our study exhibit functional performance that exceeds structural capacity predictions in certain regions (such as the prefrontal cortex), even when those regions have undergone significant atrophy. Remarkably, these regions maintain functional integrity despite structural degeneration, diverging from classical compensatory mechanisms, which typically involve

hyperactivation of intact regions to enhance task performance [5,66]. Critically, our BM metric captures this dissociation between structural decline and preserved function, highlighting a mechanism distinct from traditional compensation. This phenomenon parallels a "software upgrade" compensating for aging "hardware", where functional optimization offsets structural limitations. By quantifying BM as the gap between predicted and observed function, our framework identifies neuroplastic buffers that sustain cognition despite atrophy. These insights inform targeted interventions to amplify BM-driven plasticity, offering biomarkers to evaluate therapeutic efficacy and guide personalized strategies to mitigate cognitive decline.

Educational attainment, a widely studied proxy for reserve, is recognized as a robust protective factor against age-related cognitive decline [67]. However, in our study we observed no significant differences in BM values between high-education (≥14 years) and low-education groups within BM hubs. We posit that this finding arises from the fundamentally different mechanisms that education and our BM metric reflect: education primarily reflects early-life advantages in neurobiological "hardware" (greater structural and cognitive development capacity), whereas our BM metric captures late-life adaptive "software" mechanisms that optimize functional performance within existing structural constraints. Extensive evidence demonstrates that higher educational attainment confers broad protective effects on late-life cognition, including benefits in executive function, visuospatial skills, language, and working memory [68,69]. Higher education is also associated with reduced risk of Alzheimer's disease and dementia [70-72], with stronger benefits for attention and executive function in preclinical stages compared to dementia cohorts [73]. Critically, however, education's protective effects are attributed to elevated peak cognitive capacity in early adulthood rather than a slower rate of decline in later years [74,75]. Thus, while education helps maintain baseline cognitive performance in normal aging, it may inadequately buffer against the cognitive deterioration driven by aging or pathology. This distinction aligns with our findings: high education alone, without concurrent functional adaptation, does not augment BM. In other words, educational advantages in youth ("hardware") do not automatically translate to enhanced maintenance of function in old age ("software").

This underscores BM's unique role in quantifying resilience through real-time neural efficiency rather than static structural reserves. It offers insights for interventions targeting adaptive plasticity to mitigate aging-related decline. Taken together, these findings suggest that traditional proxies and imaging-based maintenance metrics capture partially non-overlapping mechanisms of resilience. We therefore advocate integrative models that combine conventional proxies with imaging-based indices of BM to more comprehensively characterize individual differences in late-life cognitive outcomes.

Although we observed statistically significant associations between our imaging-derived BM index and concurrent cognitive performance (with the largest effects for episodic memory), the explained variance was modest (<1.5%). We view this modest effect size as consistent with the construct our metric targets. As clarified elsewhere, the present measure is best interpreted as a brain maintenance (BM)–oriented index—capturing the contemporaneous preservation of structure–function coupling and, where deviations occur, potential adaptive efficiency—rather than as a proxy of premorbid capacity. Consequently, the index is not designed to determine absolute baseline cognition, which is influenced by multiple lifelong factors (e.g., early-life capacity, comorbidities, sensory and vascular factors). Instead, it is intended to index resilience against further decline: individuals may vary widely in current performance, yet those with higher BM index values are hypothesized to decline more slowly as aging or pathology progresses.

This interpretation also clarifies why traditional proxies such as educational attainment—strong predictors of baseline cognitive level—need not align strongly with the BM-oriented index in cross-sectional analyses. Proxies largely reflect early-life advantages ("hardware"), whereas our metric emphasizes ongoing, late-life preservation/adaptation ("software"). Thus, small cross-sectional effects should not be taken to imply limited clinical relevance. Rather, they motivate a longitudinal testable prediction: higher BM index today should forecast reduced future cognitive decline, even after accounting for baseline performance and demographic proxies. Evaluating this prediction will require repeated assessments with harmonized neuroimaging and

cognition, which we identify as a key direction for future work.

BM hubs exhibit domain-specific and domain-general contributions to multi-domain cognition. Subregions within maintenance hubs—such as the medial/lateral superior frontal gyrus, precuneus, and cingulate cortex—demonstrated both specialized and overlapping associations with distinct cognitive domains in multivariate analyses. These regions overlap extensively with the fronto-striatal circuitry, a critical network linking the prefrontal cortex with subcortical striatum to support higher-order cognitive functions through complex cross-regional interactions [76,77]. Our findings suggest that the relationship between BM and cognition depends on the differential contributions of these key subregions, with varying functional "weights" across cognitive domains. However, the specific neural mechanisms by which these subregional circuits mediate BM's effects on cognition remain to be elucidated and will be an important topic for future research. Moreover, regions with positive function–structure discrepancies (observed function > predicted) were found mainly in higher-order association cortices (e.g., frontoparietal regions). In our analytical framework, such positive deviations indicate that functional activity is being preserved or enhanced beyond what cortical atrophy alone would predict, consistent with concepts of brain maintenance [42]. This finding aligns with the posterior–anterior shift in aging, where older adults show increased frontal (anterior) activation and reduced occipital (posterior) activation as an adaptive response to neurodegeneration [78]. The elevated functional performance in these regions may reflect protective scaffolding that helps maintain cognitive function despite structural declines. In contrast, regions with negative discrepancies (observed function < predicted), including parts of the occipital cortex, likely represent areas of vulnerability where structural aging leads to a proportional loss of function, indicating less available BM capacity. These interpretations illustrate how the spatial patterns in Figure 2.a support our model's premise: they map out where the brain manages to uphold function against the odds of structural aging, and where it does not.

Notably, while BM values in domain-specific hubs showed statistically significant correlations with performance in their respective cognitive domains, the effect sizes were modest (Pearson $r < 0.2$). This raises questions about BM's robustness as a

standalone metric for explaining cross-sectional cognitive heterogeneity. However, this limitation aligns with our operational definition of BM as a dynamic buffer against decline rather than a direct correlate of baseline cognitive performance [4,79,80]. In support of this interpretation, our longitudinal analyses demonstrated that higher BM values predicted slower cognitive decline, independent of education (a proxy emphasizing early-life structural advantages). This dissociation underscores BM's unique utility in capturing adaptive resilience mechanisms that mitigate aging-related deterioration.

The concept of BM extends beyond mitigating normal age-related cognitive decline to critically regulating the risk of transitioning from normal cognitive aging [59] to pathological cognitive aging (PCA). Unlike conventional biomarkers of aging progression (e.g., gray matter volume, cortical thickness), BM values did not exhibit a smooth continuum of decline across the spectrum of cognitively normal, MCI, and AD individuals. Instead, we observed that MCI patients exhibit broader and more pronounced BM reductions in maintenance hubs, as well as greater sensitivity to changes in BM, compared to AD patients. This counterintuitive pattern may reflect stage-specific differences in neuroplastic capacity. In the early stages of pathology, such as MCI, residual brain maintenance and preserved neural resources may still support relatively preserved function, whereas at the AD stage, extensive structural damage is associated with a marked reduction in neural flexibility and the diminished capacity for functional reorganization. According to the Exploration-Selection-Refinement Model [81], cognitive processing relies on a dynamic equilibrium between task demands and brain's functional supply. In NCA, high BM enables individuals to restore or maintain this equilibrium by preserving functional supply when structural decline (reduces supply) occurs. MCI, while still processing some adaptive capacity, shows inefficient BM utilization, as evidenced by the marked BM reductions we found in the medial/lateral prefrontal cortex—key hubs for adaptive resource allocation. In contrast, AD's widespread structural damage disrupts the neural "hardware" required for BM-driven "software" optimization, rendering BM metrics unreliable in these regions. Notably, within the MCI, higher BM in the superior temporal gyrus and precuneus strongly was strongly associated with lower Aβ deposition, highlighting BM's potential

as an early biomarker for preclinical AD pathology. In summary, these results extend existing BM frameworks by operationalizing brain maintenance as preserved structure–function correspondence, providing a quantitative basis to examine individual differences in neural resilience across aging and neurodegeneration. It is important to acknowledge several methodological considerations in our BM-based prediction model for Aβ deposition. In the present study, we adopted a univariate generalized linear regression (GLM) approach with leave-one-out cross-validation (LOOCV), in which each BM-related region was evaluated independently as a predictor. This approach was chosen primarily to ensure model stability given the ratio of available sample size to the high dimensionality of regional features. By isolating each region, we were able to avoid overfitting and to obtain an interpretable measure of each region's predictive contribution. However, this strategy comes with limitations. Most notably, by treating regions independently, the model does not capture inter-regional covariance or the network-level interactions that are intrinsic to brain organization. As a result, our findings should be interpreted as indicating region-specific associations with Aβ deposition, rather than as independent contributions controlling for all other regions. Future studies with larger samples will be better positioned to implement multivariate or regularized machine learning approaches (e.g., LASSO, ridge regression, or multivariate partial least squares) to model the joint predictive value of multiple regions simultaneously, thereby taking into account the covariance structure of the brain. Despite this limitation, our univariate GLM–LOOCV framework provides a conservative and interpretable step toward identifying BM-related regions that are most strongly associated with Aβ burden, while minimizing the risk of overfitting and enhancing reproducibility in the current dataset.

Methods

Participants

Participants were from the BABRI community cohort [82], a community-based cohort of middle-aged and older adults started in 2008. The BABRI project was

approved by the Ethics Committee of the State Key Laboratory of Cognitive Neuroscience and Learning (IRB_A_0010_2024001) and the Institutional Review Board of the Brain Imaging Center of Beijing Normal University. All participants gave written informed consent.

Inclusion criteria were: (1) aged ≥50 years; (2) ≥6 years of education; [30] no diagnosis of neurodegenerative (e.g., AD, Parkinson's disease), neurological (e.g., severe cerebrovascular disease, brain tumor, trauma), or severe psychiatric disorders (e.g., major depression, bipolar disorder, schizophrenia); (4) no history of drug/alcohol abuse; (5) MMSE - Chinese version score ≥24 to exclude suspected dementia [83]; (6) physical and mental ability to complete neuropsychological tests and information collection; and (7) completed T1 - weighted MRI and resting - state fMRI scans with no contraindications and acceptable image quality.

Initially, 1,482 participants aged 50-90 were included. After excluding those who failed to meet the criteria and those with poor-quality images (incomplete scans, significant artifacts, fMRI maximum head motion > 3 mm/3°, or Mean FD > 0.5 mm), 1,280 participants remained (age: 66.45 ±7.26 years; 494 men, 786 women; education: 11.49 ±3.14 years). Among them, 323 had longitudinal cognitive assessment data (average follow-up: 3.19 ±1.34 years). All longitudinal analyses were based on two timepoints: baseline and a single follow-up assessment for each participant. The timing and distribution of follow-up visits are illustrated in Supplementary Figure 1.

A total of N = 243 healthy young adults (136 females; mean age = 18.67±1.91 years; mean education = 16.34±1.28 years were recruited to establish the youthful structural–functional reference model. This age range was selected because it corresponds to the peak of neurodevelopmental maturation and stable neuroanatomical profiles.

The participant group for studying disease-related BM characteristics was separate from the above group. A total of 135 participants were recruited, including 76 NC, 30 MCI patients, and 29 AD patients (See Supplementary Table 1). All participants completed florbetapir PET, structural MRI, and an extensive cognitive battery within a month. All participants met the following criteria: right-handed; native Chinese

speakers; at least 50 years old; and no history of neurological or psychiatric disorders. The diagnostic criteria for MCI based on Petersen's criteria included (1) the presence of subjective cognitive complaints (self-reported and/or by informants); (2) normal general cognition (a score higher than 23 on the Mini-mental State Examination [MMSE]); [30] intact daily function (a score of 0 in the Instrumental Activity of Daily Living [IADL] and ADL); and (4) objective cognitive impairment (neuropsychological tests scores in "Neuropsychological test" less than 1.5 standard deviations below the age- and education-adjusted norms of the Chinese elderly population) [84]. AD was diagnosed according to the criteria of the National Institute of Neurological and Communicative Disorders and Stroke and the Alzheimer's Disease and Related Disorders Association Dementia [85,86] and further evaluated by brain CT or MRI. All participants gave written informed consent to our protocol, which was approved by the ethics committee of the State Key Laboratory of Cognitive Neuroscience and Learning, Beijing Normal University.

Behavioral and cognitive assessment

Neuropsychological assessments were administered only to the healthy older cohort and the MCI/AD patient group, but not to the young reference cohort. These participants underwent a battery of neuropsychological tests at baseline recruitment [82]. The assessment involved general cognitive ability and cognitive function across five domains including memory, language, attention, spatial processing, and executive function. General cognitive ability was tested using the Chinese version of the MMSE [83]. Memory was tested using the Auditory Verbal Learning Test (AVLT) [87]. Executive function was tested using the Stroop Color Word Test (SCWT) [88] and the Trail Making Test (TMT-B) [89]. Spatial processing was assessed using the Clock Drawing Test (CDT) [90]. Attention was evaluated using the Symbol Digit Modification Test (SDMT) [91]and the TMT_A test [89]. Language was tested using the Boston Naming Test (BNT) and the Verbal Fluency Test (VFT) [92].

Cognitive Decline Metric

Cognitive decline was quantified based on two available neuropsychological assessments per participant (baseline and follow-up). The follow-up interval varied

across individuals (mean = 3.19 years, SD = 1.34 years, range = ~1–6 years). For each cognitive domain, we computed the annualized rate of change by dividing the difference between follow-up and baseline scores by the follow-up interval (years). This approach provides a linear approximation of decline for each participant. While limited in capturing nonlinear trajectories or short-term fluctuations, this measure allows for an overall assessment of longitudinal cognitive change across the cohort.

Network Parcellation and Assignment

To investigate the network-level distribution of BM regions, we assigned each brain region to one of seven canonical large-scale functional networks based on the Schaefer et al. 7-network parcellation scheme. The networks include: Default Mode Network (DMN), Frontoparietal Network (FPN), Ventral Attention Network (VAN), Dorsal Attention Network (DAN), Somatomotor Network (SomMot), Visual Network (Vis), Limbic Network (Limbic).

Each region-of-interest (ROI) from the brain parcellation was assigned to a network according to the atlas provided by Schaefer et al. (2018) [93]. This network assignment was used to quantify and compare the distribution of BM hubs and values across functional systems, as described in the Results.

MRI image acquisition and data processing

MRI scanning was performed in all participants. MRI data were acquired using a SIEMENS PRISMA 3T scanner at the Imaging Center for Brain Research at Beijing Normal University. Participants were in a supine position with their heads snugly fixed by straps and foam pads to minimize head movement. The T1-weighted structural images were acquired using 3D magnetization-prepared rapid gradient echo sequences: 192 sagittal slices, repetition time (TR)=2530 ms, echo time (TE)=2.27 ms, slice thickness=1 mm, flip angle (FOA)=7°, and field of view (FOV)=256 mm×256 mm. Resting-state fMRI was acquired with 33 axial slices, TR = 2000 ms, TE = 30 ms, flip angle = 90°, slice thickness = 3.5 mm, matrix = 64 × 64, and FOV = 200 × 200 mm². During scanning, participants rested with eyes closed, remained awake, and minimized head movement.

The MATLAB2021b (https://ww2.mathworks.cn/) and SPM12

(https://www.fil.ion.ucl.ac.uk/spm/software/spm12/) toolboxes with default parameters were used to pre-process the structural images. Modulated gray matter (GM) images were obtained through voxel-based morphometry and smoothed with an 8 mm full width at half maximum (FWHM) gaussian kernel to enhance signal-to-noise ratio and account for inter-individual anatomical variability, consistent with standard VBM procedures. Structural preprocessing was performed using the fMRIPrep pipeline, which applies standardized tissue probability maps in MNI space. A gray matter mask derived from these template-based priors was used to constrain subsequent analyses. For all subjects, cortical reconstruction of T1-weighted images was performed using FreeSurfer version 5.3 (http://surf er.nmr.mgh.harvard.edu) [94]. This process involved registration to a template, intensity normalization, gray/white matter segmentation, and tessellation of gray/CSF and white/gray boundaries. Cortical surfaces were inflated and normalized via spherical registration, with cortical thickness defined as the shortest distance between the pial and white matter surfaces. The average regional cortical thickness was calculated without manual correction. The procedure included bias field correction, intensity normalization, and skull stripping using a watershed algorithm, followed by white matter segmentation, surface definition, and topology correction of the reconstructed surfaces. We used a triangular surface mesh representation of the midthickness human cortical surface. This representation, comprising 163,842 vertices in each hemisphere, was obtained from a down sampled, left–right symmetric version of the FreeSurfer's fsaverage population-averaged template(https://github.com/ThomasYeoLab/CBIG/tree/master/data/templates/surface/fs_LR_164k). Note that the template is independent of the data sample used in our analyses, thus avoiding concerns about circularity.

The preprocessing pipeline for functional neuroimaging data

Resting-state fMRI scanning was performed in all participants. Resting-state fMRI data were preprocessed using fMRIPrep (https://fmriprep.org/, V20.1.3), a standardized preprocessing framework that integrates multiple neuroimaging packages, including FSL, ANTs, FreeSurfer, and AFNI [59]. The preprocessing procedure included head motion estimation, slice-timing correction, functional-to-structural registration, and

normalization to standard space. Quality control involved visual inspection of the anatomical images and exclusion of subjects with excessive head motion (maximum displacement > 3 mm or 3°, or mean framewise displacement > 0.5 mm).

Importantly, global signal regression (GSR) was not applied in the functional preprocessing pipeline used in this study. After preprocessing, each 3D BOLD volume at each TR was projected onto the cortical surface using mri_vol2surf (FreeSurfer). Surface signals were then extracted separately for the left and right hemispheres and assembled across time into hemisphere-specific vertex-by-time fMRI matrices for downstream analyses. Thus, the functional input to the structural-to-functional modeling framework consisted of cortical surface-based time series represented at the vertex level, rather than voxel-wise volumetric data.

Confound estimation was performed during preprocessing for quality assessment and standard nuisance characterization; however, no whole-brain global signal regression step was included in the pipeline used to generate the final functional matrices. Post-processing steps included linear drift removal, spatial smoothing, and temporal band-pass filtering (0.01–0.1 Hz), after which the resulting surface-based time series were used for subsequent modeling.

PET processing

PET scanning was performed only in MCI/AD patients. We used SPM12 to rigidly coregister the florbetapir PET scan to the structural MRI scan and spatially normalize it to a reference template. All PET images underwent smoothing with an 8 mm FWHM Gaussian filter. The standardized uptake value ratio (SUVR), a common semiquantitative method in antiamyloid drug trials, measures amyloid accumulation. Typically, the whole cerebellum or cerebellar gray matter serves as the reference region due to its minimal amyloid buildup [95-100]. Using the cerebellum as the reference region is based on the assumption that its amyloid accumulation is negligible. However, post-mortem studies have shown that a diffuse type of senile plaques exists in the cerebellum of some AD patients [96]; meanwhile, the longitudinal study found the subcortical white matter, such as corpus callosum was relatively unaffected by amyloid accumulation [101], and it has been shown to be a reliable reference brain region [100,102]. The use of the

cerebellum as the reference region in these cases where there is significant amyloid accumulation in the cerebellum is therefore inadequate. Thus, in the present study, we combined cerebellar GM and reliable reference brain region from longitudinal studies, that is, corpus callosum to generate average SUVR, from which the whole cerebellum was obtained from AAL, and the corpus callosum atlas came from the IIT Human Brain Atlas (https://www.nitrc.org/projects/iit) [102,103].

Statistical analysis

Cortical Reconstruction and Thickness Extraction

This study employed multimodal neuroimaging data to examine the relationship between cortical thickness and functional reorganization. For structural data, individual cortical thickness maps were reconstructed using FreeSurfer and represented on the fsaverage surface space (163,842 vertices per hemisphere), yielding a vertex-by-participant matrix for each hemisphere. For functional data, preprocessed resting-state fMRI signals were projected onto the cortical surface and organized as hemisphere-specific vertex-by-time matrices, which were then stacked across participants to form a three-dimensional functional representation of vertex × time × participant (Figure 1.a).

To characterize structure–function relationships, we adopted a revised spatiotemporal joint modeling framework. Rather than modeling each vertex or each time point independently, the functional output for each hemisphere was represented as a spatiotemporal tensor $Y \in \mathbb{R}^{V \times T}$, whereas the structural input was represented as a cortical thickness vector $x \in \mathbb{R}^{V}$. The output tensor was partitioned into spatiotemporal blocks defined jointly over local vertex blocks and temporally contiguous windows. In the revised analysis, temporally contiguous windows of 100 TRs were used as the basic temporal modeling unit. Prediction was then performed jointly within each vertex-block × time-window unit, allowing multiple vertices and multiple time points to be estimated simultaneously under a shared optimization objective.

This framework was introduced to avoid the implicit assumption that vertices and time points are mutually independent. By jointly estimating local spatial and temporal structure, the model explicitly captures both spatial covariance and temporal dependency in the resting-state fMRI signal. Importantly, the revised framework does

not assume that the same TR index across participants corresponds to the same latent neural event. Instead, each participant contributes their own within-subject temporal sequence, and the model learns mappings to temporally continuous functional windows represented in a reduced spatiotemporal space.

Measurement of BM Values

To quantify brain maintenance (BM), we developed a structural-to-functional prediction model based on vertex-level cortical thickness and resting-state fMRI data. Structural data consisted of 163,842 cortical vertices per hemisphere in fsaverage space. Functional data consisted of 240 resting-state time points per participant, forming a vertex-by-time matrix for each hemisphere.

In the cortical functional reorganization analysis, machine learning-based predictive models were employed to establish associations between vertex-level cortical thickness and functional activity patterns. prediction was performed using a leave-one-subject-out cross-validation [104] design. In the young reference group, model reliability was confirmed by achieving a robust correlation between predicted and observed resting-state functional activity ($R > 0.6$), with all permutation tests yielding $p < 1 \times 10^{-6}$. This demonstrated that the structural–functional mapping in young adults was consistent and reliable, supporting its use as a reference model for BM quantification.

To reduce overfitting under the high-dimensional setting, dimensionality reduction was carried out explicitly within each fold. Specifically, principal component analysis (PCA) was applied to the structural input using the training participants only, and the held-out participant was projected into the corresponding fold-specific low-dimensional space. A corresponding PCA procedure was also applied to the functional output using training data only, while preserving the temporal dimension. Thus, both the input and the output were represented in reduced spaces prior to prediction, substantially reducing dimensionality and preventing train–test leakage.

Within each LOSO fold, the model learned a mapping from cortical thickness to spatiotemporal functional blocks in the young reference group. This mapping was then applied to older participants without parameter re-estimation, thereby estimating the

functional patterns maximally attainable from their preserved cortical structural integrity. Importantly, the aging cohort was never used to fit or optimize the reference mapping itself. Accordingly, the resulting BM metric reflects deviation from a normative structure–function relationship defined in young adults, rather than age-specific model fitting.

The resulting mapping was subsequently applied to the elderly cohort to estimate their maximally attainable functional capacity based on cortical structural integrity. Importantly, this step involved no parameter re-estimation: cortical thickness data from older individuals were projected into a fixed reference model derived from the young cohort. Consequently, the resulting brain maintenance (BM) metric reflects deviation from a normative structure–function relationship rather than a model fitted to aging data, thereby reducing the risk of overfitting.

The framework preserves temporal structure throughout the functional representation and reconstruction process. Prediction is performed over temporally contiguous windows rather than isolated TRs, and the predicted blocks are then assembled back into a participant-specific reconstructed functional time series. Thus, the final model output is not a set of unrelated spatial states, but a temporally ordered reconstructed sequence for each participant. This distinction is critical because downstream functional connectivity (FC) analyses were derived from the reconstructed within-subject temporal series, rather than from independent spatial states lacking temporal continuity.

To quantify structure–function discrepancy, time series were extracted using the Schaefer2018 functional network parcellation template [105], and FC matrices were computed for both empirically observed and structure-predicted signals. Brain visualizations were generated using BrainNet Viewer implemented in MATLAB [106]. The discrepancy between these matrices was quantified using the Frobenius norm. In our framework, positive discrepancies (observed function exceeding reconstructed prediction) indicate regions where functional activity is maintained or enhanced beyond what cortical structure alone would predict, consistent with the concept of BM as protective adaptation. Conversely, negative discrepancies (observed function falling

below structural prediction) reflect regions where functional performance declines more than expected from structural integrity. Thus, rather than interpreting all deviations from the optimal young-adult reference as higher BM, we differentiate between *positive deviations* (empirical function > reconstructed function) and *negative deviations* (empirical function < reconstructed function). This approach allows us to capture both maintenance mechanisms within the aging brain (Figure 1.b).

SCCA Analysis

The current study used Sparse Canonical Correlation Analysis (SCCA) to explore the relationship between the spatial distribution of BM and multi-domain cognitive function. Unlike traditional CCA, which struggles with high-dimensional data, SCCA introduces regularization to handle cases where feature dimensions exceed the sample size. It has been successfully applied in neuroscience research linking neuroimaging and behavioral data [107-109]. Sparse regularization was applied in the structure–cognition analyses (SCCA), where inference depended on estimating associations between brain features and behavioral outcomes. In contrast, sparse regularization was not applied to the structure–function mapping, as no parameters were optimized in the aging cohort. Instead, the mapping function was fixed a priori, and BM was quantified as a deviation metric relative to this reference space. Therefore, regularization was not required for controlling model complexity in this context [110].

The analysis was performed in R using the PMA package. The model maximized the covariance between linear combinations of cortical thickness (u) and cognitive scores (v), while maintaining sparsity. This multivariate method effectively identifies key associations between brain reorganization and cognitive function.

To avoid overfitting and inflated covariance estimates, the study adopted a training/test split. Optimal sparsity parameters were determined via five-fold cross validation and grid search on the training set, with model performance validated on the independent test set. BM values and cognitive function canonical correlation coefficients were generated for the test set. Bonferroni correction was applied to control for multiple comparison false positives, with only features having |weights| > 0.1 reported. This design provides an unbiased estimate of BM-cognition associations.

Covariate Control and Group Comparison

Covariate effects on the primary dependent variable (BM) were controlled using multiple linear regression. Specifically, age, sex, and years of education were included as covariates and mean-centered prior to analysis. For each brain region, BM values were regressed on these covariates, and the resulting residuals were used for subsequent analyses as covariate-adjusted measures.

To prevent information leakage, covariate adjustment was performed strictly within each cross-validation fold. For each iteration, regression coefficients were estimated using only the training data and then applied to both the training and corresponding test sets to obtain covariate-adjusted residuals. This ensured that no information from the held-out data contributed to covariate estimation, in accordance with recommended best practices for predictive modeling [111].

All reported results therefore reflect fully cross-validated estimates, with covariate adjustment and model evaluation strictly separated across folds.

When comparing BM values between demographic groups (e.g., males vs. females), covariate adjustment included age and education only. Similarly, when examining the effects of age or education on BM, the remaining demographic variables were included as covariates. Group differences in BM residuals were assessed using independent-sample t-tests for the relevant brain regions (Figure1.c.①).

Cognitive Behavioral Longitudinal Dataset

Calculating Rates of Cognitive Decline

Within the large sample of 1,280 participants, 323 had longitudinal cognitive - assessment data. For each individual, the rate of decline in each cognitive domain was calculated by subtracting baseline cognitive scores from follow - up scores and dividing by the time interval (in years) between baseline and follow-up.

Correlations and Spatial Distribution of BM Values and Cognitive Decline Rates

To test if BM values correlate with cognitive decline rates, Pearson correlations were computed between the two. Brain regions with significant correlations (after correction) were marked. Additionally, we examined correlations between the summed BM values across all brain regions and cognitive decline rates to explore which

cognitive domains show stronger associations with preserved brain maintenance (Figure 1.c.②).

Pathological Aging Validation Dataset

ANOVA Analysis

Firstly, we obtained the BM values for further analysis by controlling for age, sex, and education using linear regression residuals. A one-way ANOVA was performed on the residuals of BM values across brain regions for the CN, MCI, and AD groups. Regions with significant between-group differences (FDR-corrected $p < 0.05$) were identified and further compared using Tukey's HSD test to determine which pairs (CN-MCI, CN-AD, MCI-AD) showed significant BM differences. Additionally, correlations were assessed between BM value differences (relative to the CN group mean) in these regions and cognitive differences between the MCI/AD groups and the CN group.

Building a BM-Based Prediction Model for Aβ Deposition

To evaluate whether brain maintenance (BM)–related regions carry predictive information about amyloid-β (Aβ) deposition, we implemented a univariate generalized linear regression (GLM) framework combined with LOOCV method. The steps were as follows: For each BM-related brain region, we treated the whole-brain Aβ deposition level as the target variable (Y) and the regional BM value as the predictor (X). A separate GLM was fit for each region independently, rather than entering all regions simultaneously into a multivariate model.

Predictive performance was quantified using root mean squared error (RMSE) across LOOCV folds. Rather than relying solely on the mean of the outcome variable as a baseline, prediction accuracy was interpreted relative to a permutation-informed null model. Specifically, Aβ values were randomly permuted across individuals and RMSE was recomputed under the same LOOCV procedure, yielding an empirical null distribution that reflects chance-level performance. This approach allows assessment of whether observed predictive accuracy exceeds what would be expected under random association.

To avoid circular inference, region-level screening based on RMSE was treated strictly as a data-driven feature identification step within the cross-validation

framework. No group-level statistical inference was performed at this stage. Regions exhibiting RMSE values f lower than the permutation-based null expectation were retained as candidate predictors. For these regions, inverse RMSE (1/RMSE) was used as an index of relative predictive strength (Figure 1.c.③).

Subsequently, statistical analyses of the association between BM values and Aβ deposition were conducted at the group level (training + test sets). Specifically, after predictive regions were identified using leave-one-out cross-validation (LOOCV), BM values were extracted from these regions across the entire cohort, and group-level regressions were performed to assess the relationship with global Aβ burden. These analyses were conducted post hoc and are therefore interpreted as exploratory rather than confirmatory. This analytical separation ensures that feature selection and statistical inference were not conflated, thereby reducing the risk of circularity and inflated effect sizes. Future work with independent validation cohorts or nested cross-validation will be necessary to establish the generalizability of these associations.

Several limitations of this study should be acknowledged. Most importantly, the absence of longitudinal neuroimaging data in pathological aging cohorts restricts our ability to delineate how BM dynamically mitigates pathological progression or modulates the transition risk from normal to pathological aging. While such data allow us to quantify structure–function discrepancies and their associations with cognition and pathology at the group level, they cannot capture the dynamic processes through which brain maintenance are engaged as structural decline unfolds over time. Indeed, prior longitudinal studies [2,7,112,113] demonstrate that repeated assessments are essential for directly probing the temporal dynamics of maintenance. Future work applying our structure-informed maintenance index in longitudinal cohorts will therefore be critical to validate and extend our findings, and to track how individual differences in maintenance evolve in relation to cognitive decline and disease progression.

Second, although longitudinal cognitive assessments were available for a subset of participants (n = 323), the relatively limited follow-up interval (mean follow-up: 3.19 ±1.34 years) and incomplete coverage of behavioral domains constrain causal inferences between regarding the protective effects of maintenance and their

relationship to cognitive decline. Extended follow-up studies incorporating serial multimodal neuroimaging (e.g., annual MRI/PET) alongside comprehensive cognitive testing will be critical to establish the temporal neuroprotective effects of maintenance and to unravel the bidirectional relationships between maintenance, structural atrophy, and pathological spread.

Third, a key limitation of the present study is that our cognitive decline metric was derived from only two time points per participant collected at variable follow-up intervals. As such, the estimated "rate of change" should be interpreted as a simplified, linear index of decline between baseline and follow-up, rather than a robust trajectory. This method does not account for potential nonlinear patterns of decline, intra-individual variability, or short-term fluctuations in cognition. Furthermore, heterogeneity in follow-up duration introduces additional variability that may reduce precision. Nevertheless, this approach provides a useful index of longitudinal change and enabled us to examine the association between our imaging-based maintenance index and cognitive decline. Future studies with longer follow-up durations and multiple repeated assessments will be important for validating these findings and for applying more sophisticated statistical models, such as mixed-effects models or latent growth models, to better characterize the dynamics of decline.

Finally, the exclusion of complementary biomarkers, such as tau pathology (e.g., tau-PET) or cerebral metabolism (e.g., FDG-PET), limits the biological interpretability of BM mechanisms. Future studies should integrate multi-modal neuroimaging to disentangle how BM interacts with hallmark Alzheimer's pathologies (Aβ/tau) and metabolic dysregulation.

Addressing these gaps will advance BM from a theoretical construct to a multidimensional biomarker system, bridging molecular, structural, functional, and behavioral layers of cognitive resilience. This integrative approach is essential for developing precision interventions that target BM-specific pathways to delay or prevent pathological aging.

Data availability

The minimum dataset necessary to interpret, verify, and extend the findings of this study is available under controlled access because it contains participant-level neuroimaging and/or clinical data subject to ethical, legal, and institutional restrictions. Access may be granted to qualified researchers for non-commercial academic research purposes upon application to Xin Li, Beijing normal University, lixin99@bnu.edu.cn, subject to approval by data access committee and, where required, a data use agreement. Requests will typically be reviewed within 8 weeks. Approved data will remain available to the requester for 6 months.

Code availability

Custom codes are available at https://github.com/Rainmon2020/Cognitive-Reserve.

Reference

1 Chang, D. *et al.* Older is order: entropy reduction in cortical spontaneous activity marks healthy aging. *BMC Neurosci* **25**, 74, doi:10.1186/s12868-024-00916-6 (2024).

2 Nyberg, L., Lovden, M., Riklund, K., Lindenberger, U. & Backman, L. Memory aging and brain maintenance. *Trends Cogn Sci* **16**, 292-305, doi:10.1016/j.tics.2012.04.005 (2012).

3 Nyberg, L. & Pudas, S. Successful Memory Aging. *Annu Rev Psychol* **70**, 219-243, doi:10.1146/annurev-psych-010418-103052 (2019).

4 Stern, Y. *et al.* Whitepaper: Defining and investigating cognitive reserve, brain reserve, and brain maintenance. *Alzheimers Dement* **16**, 1305-1311, doi:10.1016/j.jalz.2018.07.219 (2020).

5 Cabeza, R. *et al.* Maintenance, reserve and compensation: the cognitive neuroscience of healthy ageing. *Nat Rev Neurosci* **19**, 701-710, doi:10.1038/s41583-018-0068-2 (2018).

6 Nyberg, L. *et al.* Biological and environmental predictors of heterogeneity in neurocognitive ageing: Evidence from Betula and other longitudinal studies. *Ageing Res Rev* **64**, 101184, doi:10.1016/j.arr.2020.101184 (2020).

7 Nyberg, L. *et al.* Longitudinal stability in working memory and frontal activity in relation to general brain maintenance. *Sci Rep* **12**, 20957, doi:10.1038/s41598-022-25503-9 (2022).

8 Whitmore, L. & Beck, D. Current challenges and future directions for brain age prediction in children and adolescents. *Nat Commun* **16**, 7771, doi:10.1038/s41467-025-63222-7 (2025).

9 Kremen, W. S. *et al.* Cognitive Reserve and Related Constructs: A Unified Framework Across Cognitive and Brain Dimensions of Aging. *Front Aging Neurosci* **14**, 834765, doi:10.3389/fnagi.2022.834765 (2022).

10 Samu, D. *et al.* Preserved cognitive functions with age are determined by domain-dependent shifts in network responsivity. *Nat Commun* **8**, 14743, doi:10.1038/ncomms14743 (2017).

11 Jauny, G. *et al.* Linking structural and functional changes during aging using multilayer brain network analysis. *Commun Biol* **7**, 239, doi:10.1038/s42003-024-05927-x (2024).

12 Winkler, A. M. *et al.* Cortical thickness or grey matter volume? The importance of selecting the phenotype for imaging genetics studies. *Neuroimage* **53**, 1135-1146, doi:10.1016/j.neuroimage.2009.12.028 (2010).

13 Jirsa, V. K. & Haken, H. Field theory of electromagnetic brain activity. *Physical review letters* **77**, 960 (1996).

14 Robinson, P. A., Rennie, C. J. & Wright, J. J. Propagation and stability of waves of electrical activity in the cerebral cortex. *Physical Review E* **56**, 826 (1997).

15 Teo, P. C., Sapiro, G. & Wandell, B. A. Creating connected representations of cortical gray matter for functional MRI visualization. *IEEE transactions on medical imaging* **16**, 852-863 (1997).

16 Pang, J. C. *et al.* Geometric constraints on human brain function. *Nature* **618**, 566-574, doi:10.1038/s41586-023-06098-1 (2023).

17 Zamani Esfahlani, F., Faskowitz, J., Slack, J., Misic, B. & Betzel, R. F. Local structure-function relationships in human brain networks across the lifespan. *Nat Commun* **13**, 2053, doi:10.1038/s41467-022-29770-y (2022).

18 Park, H. J. & Friston, K. Structural and functional brain networks: from connections to cognition. *Science* **342**, 1238411, doi:10.1126/science.1238411 (2013).

19 Valenzuela, M. J. & Sachdev, P. Brain reserve and dementia: a systematic review. *Psychol Med* **36**, 441-454, doi:10.1017/S0033291705006264 (2006).

20 Fratiglioni, L. & Wang, H.-X. Brain reserve hypothesis in dementia. *Journal of Alzheimer's disease* **12**, 11-22 (2007).

21 Sun, L. *et al.* Human lifespan changes in the brain's functional connectome. *Nat Neurosci* **28**, 891-901, doi:10.1038/s41593-025-01907-4 (2025).

22 Bethlehem, R. A. I. *et al.* Brain charts for the human lifespan. *Nature* **604**, 525-533, doi:10.1038/s41586-022-04554-y (2022).

23 Foulkes, L. & Blakemore, S. J. Studying individual differences in human adolescent brain development. *Nat Neurosci* **21**, 315-323, doi:10.1038/s41593-018-0078-4 (2018).

24 Deco, G., Jirsa, V. K. & McIntosh, A. R. Emerging concepts for the dynamical organization of resting-state activity in the brain. *Nature reviews neuroscience* **12**, 43-56 (2011).

25 Arenaza-Urquijo, E. M. *et al.* Sex and gender differences in cognitive resilience to aging and Alzheimer's disease. *Alzheimers Dement* **20**, 5695-5719, doi:10.1002/alz.13844 (2024).

26 Boyle, C. P. *et al.* Estrogen, brain structure, and cognition in postmenopausal women.

Hum Brain Mapp **42**, 24-35, doi:10.1002/hbm.25200 (2021).

27 Caselli, R. J. *et al.* Sex-based memory advantages and cognitive aging: a challenge to the cognitive reserve construct? *J Int Neuropsychol Soc* **21**, 95-104, doi:10.1017/S1355617715000016 (2015).

28 Diaz-Caneja, C. M. *et al.* Sex Differences in Lifespan Trajectories and Variability of Human Sulcal and Gyral Morphology. *Cereb Cortex* **31**, 5107-5120, doi:10.1093/cercor/bhab145 (2021).

29 Febo, M. *et al.* Longitudinal Characterization and Biomarkers of Age and Sex Differences in the Decline of Spatial Memory. *Front Aging Neurosci* **12**, 34, doi:10.3389/fnagi.2020.00034 (2020).

30 Long, M. A. *et al.* Functional Segregation of Cortical Regions Underlying Speech Timing and Articulation. *Neuron* **89**, 1187-1193, doi:10.1016/j.neuron.2016.01.032 (2016).

31 Cole, M. W., Yarkoni, T., Repovš, G., Anticevic, A. & Braver, T. S. Global connectivity of prefrontal cortex predicts cognitive control and intelligence. *Journal of Neuroscience* **32**, 8988-8999 (2012).

32 Freedberg, M. V. The balance of hippocampal and caudate network functional connectivity is associated with episodic memory performance and its decline across adulthood. *Neuropsychologia* **191**, 108723 (2023).

33 Kizilirmak, J. M. *et al.* The relationship between resting-state amplitude fluctuations and memory-related deactivations of the default mode network in young and older adults. *Human Brain Mapping* **44**, 3586-3609 (2023).

34 Deery, H. A., Di Paolo, R., Moran, C., Egan, G. F. & Jamadar, S. D. The older adult brain is less modular, more integrated, and less efficient at rest: A systematic review of large-scale resting-state functional brain networks in aging. *Psychophysiology* **60**, e14159 (2023).

35 Deery, H. A. *et al.* Reconfiguration of metabolic connectivity in ageing. *Communications Biology* **7**, 1600 (2024).

36 Filippi, M. *et al.* Age-related vulnerability of the human brain connectome. *Molecular Psychiatry* **28**, 5350-5358 (2023).

37 Raz, N., Ghisletta, P., Rodrigue, K. M., Kennedy, K. M. & Lindenberger, U. Trajectories of brain aging in middle-aged and older adults: regional and individual differences. *Neuroimage* **51**, 501-511 (2010).

38 Tucker-Drob, E. M. Cognitive aging and dementia: a life-span perspective. *Annual review of developmental psychology* **1**, 177-196 (2019).

39 Tucker-Drob, E. M., Brandmaier, A. M. & Lindenberger, U. Coupled cognitive changes in adulthood: A meta-analysis. *Psychological bulletin* **145**, 273 (2019).

40 Stern, Y. An approach to studying the neural correlates of reserve. *Brain Imaging Behav* **11**, 410-416, doi:10.1007/s11682-016-9566-x (2017).

41 Gazes, Y. *et al.* White matter tract covariance patterns predict age-declining cognitive abilities. *NeuroImage* **125**, 53-60 (2016).

42 Habeck, C. *et al.* Cognitive Reserve and Brain Maintenance: Orthogonal Concepts in Theory and Practice. *Cereb Cortex* **27**, 3962-3969, doi:10.1093/cercor/bhw208 (2017).

43 Johansson, J. *et al.* Model of brain maintenance reveals specific change-change association between medial-temporal lobe integrity and episodic memory. *Aging Brain* **2**, 100027, doi:10.1016/j.nbas.2021.100027 (2022).

44 Steffener, J., Brickman, A. M., Rakitin, B. C., Gazes, Y. & Stern, Y. The impact of age-related changes on working memory functional activity. *Brain imaging and behavior* **3**, 142-153 (2009).

45 Maesawa, S. *et al.* Resting State Networks Related to the Maintenance of Good Cognitive Performance During Healthy Aging. *Front Hum Neurosci* **15**, 753836, doi:10.3389/fnhum.2021.753836 (2021).

46 Goldberg, E. & Bilder, R. M. in *The frontal lobes revisited* 159-187 (Psychology Press, 2019).

47 Stuss, D. T. & Benson, D. F. in *The frontal lobes revisited* 141-158 (Psychology Press, 2019).

48 Taren, A. A., Venkatraman, V. & Huettel, S. A. A parallel functional topography between medial and lateral prefrontal cortex: evidence and implications for cognitive control. *Journal of Neuroscience* **31**, 5026-5031 (2011).

49 Kozlovskiy, S. A., Nikonova, E. Y., Pyasik, M. M. & Velichkovsky, B. M. The cingulate cortex and human memory processes. *Psychology in Russia* **5**, 231 (2012).

50 Stevens, F. L., Hurley, R. A. & Taber, K. H. Anterior cingulate cortex: unique role in cognition and emotion. *The Journal of neuropsychiatry and clinical neurosciences* **23**, 121-125 (2011).

51 Dadario, N. B. & Sughrue, M. E. The functional role of the precuneus. *Brain* **146**, 3598-3607 (2023).

52 Utevsky, A. V., Smith, D. V. & Huettel, S. A. Precuneus is a functional core of the default-mode network. *Journal of Neuroscience* **34**, 932-940 (2014).

53 Margulies, D. S. *et al.* Situating the default-mode network along a principal gradient of macroscale cortical organization. *Proceedings of the National Academy of Sciences* **113**, 12574-12579 (2016).

54 Fjell, A. M. *et al.* One-year brain atrophy evident in healthy aging. *Journal of Neuroscience* **29**, 15223-15231 (2009).

55 Fjell, A. M. *et al.* What is normal in normal aging? Effects of aging, amyloid and Alzheimer's disease on the cerebral cortex and the hippocampus. *Progress in neurobiology* **117**, 20-40 (2014).

56 Fjell, A. M. *et al.* Brain changes in older adults at very low risk for Alzheimer's disease. *Journal of Neuroscience* **33**, 8237-8242 (2013).

57 Buckner, R. L. Memory and executive function in aging and AD: multiple factors that cause decline and reserve factors that compensate. *Neuron* **44**, 195-208 (2004).

58 Buckner, R. L. & DiNicola, L. M. The brain's default network: updated anatomy, physiology and evolving insights. *Nature reviews neuroscience* **20**, 593-608 (2019).

59 Esteban, O. *et al.* fMRIPrep: a robust preprocessing pipeline for functional MRI. *Nature methods* **16**, 111-116 (2019).

60 Yang, Y. *et al.* Successful or pathological cognitive aging? Converging into a" frontal preservation, temporal impairment (FPTI)" hypothesis. *Science bulletin* **67**, 2285-2290 (2022).

61 Barulli, D. & Stern, Y. Efficiency, capacity, compensation, maintenance, plasticity: emerging concepts in cognitive reserve. *Trends Cogn Sci* **17**, 502-509, doi:10.1016/j.tics.2013.08.012 (2013).

62 Gutchess, A. Plasticity of the aging brain: new directions in cognitive neuroscience. *Science* **346**, 579-582 (2014).

63 Greenwood, P. M. Functional plasticity in cognitive aging: review and hypothesis. *Neuropsychology* **21**, 657 (2007).

64 Bishop, N. A., Lu, T. & Yankner, B. A. Neural mechanisms of ageing and cognitive decline. *Nature* **464**, 529-535 (2010).

65 Grady, C. The cognitive neuroscience of ageing. *Nature Reviews Neuroscience* **13**, 491-505 (2012).

66 Reuter-Lorenz, P. A. & Cappell, K. A. Neurocognitive aging and the compensation hypothesis. *Current directions in psychological science* **17**, 177-182 (2008).

67 Satz, P., Cole, M. A., Hardy, D. J. & Rassovsky, Y. Brain and cognitive reserve: mediator (s) and construct validity, a critique. *Journal of clinical and experimental neuropsychology* **33**, 121-130 (2011).

68 Kobayashi, T. *et al.* Principles of early human development and germ cell program from conserved model systems. *Nature* **546**, 416-420 (2017).

69 Opdebeeck, C., Martyr, A. & Clare, L. Cognitive reserve and cognitive function in healthy older people: a meta-analysis. *Aging, Neuropsychology, and Cognition* **23**, 40-60 (2016).

70 Hendrie, H. C. *et al.* The association of early life factors and declining incidence rates of dementia in an elderly population of African Americans. *The Journals of Gerontology: Series B* **73**, S82-S89 (2018).

71 Manly, J. J. *et al.* Estimating the prevalence of dementia and mild cognitive impairment in the US: the 2016 health and retirement study harmonized cognitive assessment protocol project. *JAMA neurology* **79**, 1242-1249 (2022).

72 Sando, S. B. *et al.* Risk-reducing effect of education in Alzheimer's disease. *International Journal of Geriatric Psychiatry: A journal of the psychiatry of late life and allied sciences* **23**, 1156-1162 (2008).

73 Groot, C. *et al.* Differential effects of cognitive reserve and brain reserve on cognition in Alzheimer disease. *Neurology* **90**, e149-e156 (2018).

74 Lovden, M., Fratiglioni, L., Glymour, M. M., Lindenberger, U. & Tucker-Drob, E. M. Education and Cognitive Functioning Across the Life Span. *Psychol Sci Public Interest* **21**, 6-41, doi:10.1177/1529100620920576 (2020).

75 Nyberg, L. *et al.* Educational attainment does not influence brain aging. *Proc Natl Acad Sci U S A* **118**, doi:10.1073/pnas.2101644118 (2021).

76 Averbeck, B. & O'Doherty, J. P. Reinforcement-learning in fronto-striatal circuits. *Neuropsychopharmacology* **47**, 147-162, doi:10.1038/s41386-021-01108-0 (2022).

77 Kleerekooper, I. *et al.* The effect of aging on fronto-striatal reactive and proactive inhibitory control. *NeuroImage* **132**, 51-58 (2016).

78 Festini, S. B., Zahodne, L. & Reuter-Lorenz, P. A. in *Oxford research encyclopedia of psychology* (2018).

79 Stern, Y. *et al.* A framework for concepts of reserve and resilience in aging. *Neurobiol*

Aging **124**, 100-103, doi:10.1016/j.neurobiolaging.2022.10.015 (2023).

80 Stern, Y. *et al.* Mechanisms underlying resilience in ageing. *Nat Rev Neurosci* **20**, 246, doi:10.1038/s41583-019-0138-0 (2019).

81 Lindenberger, U. & Lövdén, M. Brain plasticity in human lifespan development: the exploration–selection–refinement model. *Annual Review of Developmental Psychology* **1**, 197-222 (2019).

82 Yang, C. *et al.* Early prevention of cognitive impairment in the community population: The Beijing Aging Brain Rejuvenation Initiative. *Alzheimers Dement* **17**, 1610-1618, doi:10.1002/alz.12326 (2021).

83 Zhang, M. *et al.* The prevalence of dementia and Alzheimer's disease in Shanghai, China: impact of age, gender, and education. *Annals of Neurology: Official Journal of the American Neurological Association and the Child Neurology Society* **27**, 428-437 (1990).

84 Petersen, R. C. Mild cognitive impairment as a diagnostic entity. *Journal of internal medicine* **256**, 183-194 (2004).

85 McKhann, G. *et al.* Clinical diagnosis of Alzheimer's disease: Report of the NINCDS-ADRDA Work Group* under the auspices of Department of Health and Human Services Task Force on Alzheimer's Disease. *Neurology* **34**, 939-939 (1984).

86 Dubois, B. *et al.* Revising the definition of Alzheimer's disease: a new lexicon. *The Lancet Neurology* **9**, 1118-1127 (2010).

87 Guo, Q. H., Lu, C. Z. & Hong, Z. Auditory verbal memory test in Chinese elderly. *Chinese Mental Health Journal* **15**, 13-15 (2001).

88 Guo, Q. H. *et al.* Application of Stroop color-word test on Chinese elderly patients with mild cognitive impairment and mild Alzheimer's dementia. *Chinese Journal of Neuromedicine* **4**, 701-704 (2005).

89 Reitan, R. The validity of the trail making test as an indicator of organic brain damage. *Perceptual and Motor skills* **8**, 271-176 (1958).

90 Rouleau, I., Salmon, D. P., Butters, N., Kennedy, C. & McGuire, K. Quantitative and qualitative analyses of clock drawings in Alzheimer's and Huntington's disease. *Brain and cognition* **18**, 70-87 (1992).

91 Sheridan, L. K. *et al.* Normative Symbol Digit Modalities Test performance in a community-based sample. *Archives of clinical neuropsychology* **21**, 23-28 (2006).

92 Guo, Q. H., Hong, Z. & Shi, W. X. Boston Naming Test in Chinese elderly, patient with mild cognitive impairment and Alzheimer's dementia. *Chinese Mental Health Journal* **20**, 81 (1991).

93 Schaefer, A. *et al.* Local-Global Parcellation of the Human Cerebral Cortex from Intrinsic Functional Connectivity MRI. *Cereb Cortex* **28**, 3095-3114, doi:10.1093/cercor/bhx179 (2018).

94 Fischl, B. FreeSurfer. *Neuroimage* **62**, 774-781 (2012).

95 Lopresti, B. J. *et al.* Simplified quantification of Pittsburgh Compound B amyloid imaging PET studies: a comparative analysis. *Journal of Nuclear Medicine* **46**, 1959-1972 (2005).

96 Wong, K.-P. *et al.* Quantitative analysis of [18 F] FDDNP PET using subcortical white matter as reference region. *European journal of nuclear medicine and*

molecular imaging **37**, 575-588 (2010).

97 Villemagne, V. L. & Rowe, C. C. Amyloid imaging. *International psychogeriatrics* **23**, S41-S49 (2011).

98 Huang, K.-L. *et al.* Regional amyloid deposition in amnestic mild cognitive impairment and Alzheimer's disease evaluated by [18F] AV-45 positron emission tomography in Chinese population. *PloS one* **8**, e58974 (2013).

99 Sperling, R. A. *et al.* Amyloid deposition detected with florbetapir F 18 (18F-AV-45) is related to lower episodic memory performance in clinically normal older individuals. *Neurobiology of aging* **34**, 822-831 (2013).

100 Shokouhi, S. *et al.* Reference tissue normalization in longitudinal 18 F-florbetapir positron emission tomography of late mild cognitive impairment. *Alzheimer's research & therapy* **8**, 1-12 (2016).

101 Thal, D. R., Rüb, U., Orantes, M. & Braak, H. Phases of Aβ-deposition in the human brain and its relevance for the development of AD. *Neurology* **58**, 1791-1800 (2002).

102 Chen, K. *et al.* Improved power for characterizing longitudinal amyloid-β PET changes and evaluating amyloid-modifying treatments with a cerebral white matter reference region. *Journal of Nuclear Medicine* **56**, 560-566 (2015).

103 Qi, X. & Arfanakis, K. Regionconnect: Rapidly extracting standardized brain connectivity information in voxel-wise neuroimaging studies. *Neuroimage* **225**, 117462 (2021).

104 Hadjiabadi, D. *et al.* Maximally selective single-cell target for circuit control in epilepsy models. *Neuron* **109**, 2556-2572 e2556, doi:10.1016/j.neuron.2021.06.007 (2021).

105 Schaefer, A. *et al.* Local-global parcellation of the human cerebral cortex from intrinsic functional connectivity MRI. *Cerebral cortex* **28**, 3095-3114 (2018).

106 Xia, M., Wang, J. & He, Y. BrainNet Viewer: A Network Visualization Tool for Human Brain Connectomics. *PLoS ONE* **8**, doi:10.1371/journal.pone.0068910 (2013).

107 Xia, C. H. *et al.* Linked dimensions of psychopathology and connectivity in functional brain networks. *Nat Commun* **9**, 3003, doi:10.1038/s41467-018-05317-y (2018).

108 Du, L. *et al.* Structured sparse canonical correlation analysis for brain imaging genetics: an improved GraphNet method. *Bioinformatics* **32**, 1544-1551, doi:10.1093/bioinformatics/btw033 (2016).

109 Ing, A. *et al.* Identification of neurobehavioural symptom groups based on shared brain mechanisms. *Nat Hum Behav* **3**, 1306-1318, doi:10.1038/s41562-019-0738-8 (2019).

110 Varoquaux, G. Cross-validation failure: Small sample sizes lead to large error bars. *Neuroimage* **180**, 68-77, doi:10.1016/j.neuroimage.2017.06.061 (2018).

111 Rosenblatt, M., Tejavibulya, L., Jiang, R., Noble, S. & Scheinost, D. Data leakage inflates prediction performance in connectome-based machine learning models. *Nat Commun* **15**, 1829, doi:10.1038/s41467-024-46150-w (2024).

112 Pudas, S., Josefsson, M., Rieckmann, A. & Nyberg, L. Longitudinal Evidence for Increased Functional Response in Frontal Cortex for Older Adults with Hippocampal

Atrophy and Memory Decline. *Cereb Cortex* **28**, 936-948, doi:10.1093/cercor/bhw418 (2018).

113 Fjell, A. M. *et al.* Reevaluating the role of education on cognitive decline and brain aging in longitudinal cohorts across 33 Western countries. *Nat Med*, doi:10.1038/s41591-025-03828-y (2025).

Table 1. Characteristics and neuropsychologic test results

	Large-sample Dataset	Longitudinal Dataset	Pathological aging verification dataset			
	Total	Total	Total	NC	MCI	AD
	n = 1280	n = 323	n = 135	n = 76	n = 30	n = 29
Sex (female, %)	786 (61.4%)	198 (61.3%)	79 (58.5%)	43 (56.6%)	15 (50%)	21 (72.4%)
Age (years)	66.45±7.26	65.74±6.73	68.23 ± 8.09	67.08 ± 7.63	68.73 ± 8.35	70.72 ± 8.65
Education (years)	11.49±3.14	11.47±2.98	12.60 ± 3.80	13.19 ± 3.56	12.07 ± 3.35	11.62 ± 4.62
MMSE	27.34±2.35	27.63±2.03	24.11 ± 6.96	27.58 ± 1.65	26.30 ± 1.56	12.76 ± 7.11
AVLT (N1-N5)	27.88±9.44	28.98±9.22	21.63 ± 12.20	29.08 ± 8.90	16.90 ± 8.15	6.46 ± 4.68
SDMT	34.31±10.77	34.02±10.30	29.25 ± 14.42	35.86 ± 11.50	25.16 ± 9.99	10.19 ± 8.59
TMT-A	60.23±23.03	59.18±21.72	75.77 ± 42.87	58.74 ± 20.43	86.70 ± 39.95	140.20± 62.69
TMT-B	172.44±70.99	168.46±62.61	179.10 ± 79.07	153.58 ± 50.42	210.61 ± 92.43	311.25± 89.11
SCWT C-B time	40.67±21.05	40.17±22.09	51.94±39.18	42.20±18.80	57.93±36.95	89.73±79.38
CDT	24.33±4.81	24.05±4.85	21.74 ± 8.62	25.29 ± 4.46	23.83 ± 5.51	10.07 ± 9.67
CVFT	44.61±8.99	45.65±8.76	35.77 ± 14.35	43.82 ± 8.65	34.70 ± 9.22	15.79 ± 10.33
DST	12.25±2.20	12.20±2.10	11.5±3.20	12.52±2.68	11.67±1.90	8.61±3.88

Note: The measured data are represented by the mean and standard deviation. AVLT: Auditory Verbal Learning Test; SCWT C-B: Stroop Color and Word Test

C minus Stroop Color and Word Test B (time); TMT: Trail Making Test; CDT: Clock-Drawing Test; CVFT: Category Verbal Fluency Test, including fruit, vegetable, and animal fluency test; SDMT: Symbol Digit Modalities Test; DST: Digit Span Test.

Figure 1. Methodological Framework for BM Quantification and Analysis. (a) Multimodal neuroimaging data processing pipeline. Structural MRI data underwent cortical reconstruction and cortical thickness mapping using FreeSurfer in fsaverage space. Resting-state fMRI data were preprocessed and registered to fsaverage space to generate vertex-wise functional matrices (vertex × time × participant).
(b) Machine learning-based BM measurement. Decision tree regression models linked vertex-level cortical thickness to resting-state functional activity patterns in young adults using leave-one-out cross-validation (LOOCV). Model-derived functional predictions for older adults were compared with empirical data using the Frobenius norm of connectivity matrix differences to quantify BM.
(c) Analytical modules. ① Sparse canonical correlation analysis (SCCA) with ℓ1 regularization was used to identify multivariate associations between BM spatial distribution and multidomain cognitive performance. ② Pearson correlations were used to examine associations between aggregated BM values and domain-specific cognitive decline rates. ③ Leave-one-out cross-validated regression identified BM hubs predictive of amyloid-β (Aβ) deposition, weighted by root mean squared error (RMSE) reduction.
SCCA, sparse canonical correlation analysis; LOOCV, leave-one-out cross-validation; RMSE, root mean squared error; Aβ, amyloid-β; MMSE, Mini-Mental State Examination; AVLT, Auditory Verbal Learning Test; SDMT, Symbol Digit Modalities Test; TMT-A/B, Trail Making Test A/B; SCWT, Stroop Color Word Test; CDT, Clock Drawing Test; VFT, Verbal Fluency Test; DST, Digit Span Test.

Figure 2. Spatial Distribution and Functional Architecture of Core BM Regions. (a) Whole-brain spatial distribution of BM values, showing an anterior–posterior gradient with enriched BM in prefrontal, temporal, cingulate and parietal regions.

(b) Population frequency map highlighting brain regions consistently classified as BM hubs across individuals.

(c) Positive correlation between regional BM values and hub frequency, validating the overlap between BM-rich areas and high-frequency hubs.

(d) Spatially consistent core BM regions identified by intersecting regions with high BM values and high hub frequency.

(e) Functional network decomposition of core BM regions.

(f) Ranking of canonical functional networks by total BM magnitude. Default mode, ventral attention and frontoparietal networks contributed most strongly to the BM-rich regions.

Color bars indicate the corresponding mapped variable in each panel. DMN, default mode network; VAN, ventral attention network; FPN, frontoparietal network; DAN, dorsal attention network; SomMot, somatomotor network; Vis, visual network; Limbic, limbic network. Figures were generated using MATLAB (MathWorks, Natick, MA, USA).

Figure 3. Age and Sex Differences in BM Networks. (a) Regional age differences in BM. Younger-old adults showed higher BM in prefrontal and sensorimotor regions, whereas older-old adults showed relatively higher BM in temporal and parahippocampal regions.

(b) Regional sex differences in BM. Females showed higher BM in cingulate–precuneus and frontal regions, whereas males showed higher BM in frontotemporal and parahippocampal regions.

(c) Network-level age differences in BM. Younger-old adults showed higher BM in ventral attention, somatomotor, frontoparietal and dorsal attention networks, but lower BM in visual and limbic networks than older-old adults.

(d) Network-level sex differences in BM. Males showed higher BM in default mode, frontoparietal and limbic networks, whereas females showed higher BM in somatomotor and dorsal attention networks.

Bars in c and d represent normalized BM values. Color bars indicate the mapped BM-related measure in a and b. *$p < 0.05$, ** $p < 0.01$, ***$p < 0.001$; all statistical tests were two-sided and P values were corrected for multiple comparisons. DMN, default mode network; FPN, frontoparietal network; VAN, ventral attention network; DAN, dorsal attention network; SomMot, somatomotor network; Vis, visual network; Limbic, limbic network. Figures were generated using MATLAB (MathWorks, Natick, MA, USA).

Figure 4. Domain-Specific and Cross-Phenotype Integration of BM Networks. (a) Spatial maps of BM hubs associated with distinct cognitive phenotypes. Processing speed was associated with the right supramarginal gyrus (SMG), middle cingulate cortex (MCC) and left precuneus (PCUN); episodic memory with bilateral superior frontal gyrus (SFG), left MCC and medial SFG; cognitive control with inferior orbital frontal cortex (IOFC) and anterior cingulate cortex (ACC); and working memory with the right middle temporal gyrus (MTG) and PCUN. Shared hubs across phenotypes are indicated in the panel.

(b) Contribution weights of neuropsychological tests to the four cognitive phenotypes derived from sparse canonical correlation analysis.

(c) Correlations between summed BM values of phenotype-specific hubs and composite cognitive scores weighted by neuropsychological test contributions. Pearson correlation tests were two-sided, and P values were corrected for multiple comparisons. Exact P values are shown in the panel where possible.

SMG, supramarginal gyrus; MCC, middle cingulate cortex; PCUN, precuneus; SFG, superior frontal gyrus; IOFC, inferior orbital frontal cortex; ACC, anterior cingulate cortex; MTG, middle temporal gyrus. Figures were generated using MATLAB (MathWorks, Natick, MA, USA).

Figure 5. BM Networks Predict Slowed Cognitive Decline in Aging. (a, c) Spatial distribution of BM hubs associated with reduced decline rates across cognitive domains. Stronger protective effects were observed for general cognition and working memory, followed by visuospatial and language domains, whereas episodic memory, processing speed and cognitive control showed more restricted phenotype-specific associations.

(b, d) Negative correlations between aggregated BM values, summed across decline-related hubs, and cognitive decline rates. Higher BM was associated with slower longitudinal cognitive deterioration. Pearson correlation tests were two-sided, and P values were corrected for multiple comparisons. Exact P values are shown in the panels where possible.

Color bars indicate the mapped BM-related measure in a and c. MMSE, Mini-Mental State Examination; DST, Digit Span Test; CDT, Clock

Drawing Test; VFT, Verbal Fluency Test; AVLT, Auditory Verbal Learning Test; TMT-A, Trail Making Test A; SCWT, Stroop Color Word Test. Figures were generated using MATLAB (MathWorks, Natick, MA, USA).

Figure 6. Stage-Specific Vulnerability of BM in Pathological Aging. (a) Whole-brain spatial BM patterns in cognitively normal (CN), mild cognitive impairment [24] and Alzheimer's disease (AD) groups.

(b) Summed BM values across BM-related regions in CN (n = 76), MCI (n = 30) and AD (n = 29) participants. Violin plots show the distribution of BM values; center lines indicate the median, boxes indicate the interquartile range and whiskers indicate the minima and maxima. Group differences were assessed using one-way ANOVA followed by Tukey's honestly significant difference (HSD) post hoc tests. All statistical tests were two-sided. *$p < 0.05$, ** $p < 0.01$, *** $p < 0.001$; P values were corrected for multiple comparisons. Exact P values are provided where possible.

(c) Network-level BM differences across pathological aging groups. Bars represent mean values ± SEM. *$p < 0.05$, ** $p < 0.01$, *** $p < 0.001$; all statistical tests were two-sided and P values were corrected for multiple comparisons.

(d) Spatial maps of BM reductions in MCI versus CN and AD versus CN.

(e) Overlap and specificity of BM-deficient regions across disease stages.

(f) Associations between BM deficits in MCI/AD and domain-specific cognitive performance. Pearson correlation tests were two-sided, and P

values were corrected for multiple comparisons. Exact P values are shown in the panels where possible.

Color bars indicate the corresponding mapped variable in a, d and e. CN, cognitively normal; MCI, mild cognitive impairment; AD, Alzheimer's disease; DMN, default mode network; VAN, ventral attention network; FPN, frontoparietal network; SEM, standard error of the mean. Panels a–d and f were generated using MATLAB (MathWorks, Natick, MA, USA). Panel e was generated using Python.

Figure 7. Stage-Specific Predictive Efficacy of BM Networks for Aβ Deposition. (a) Regional predictive power of BM hubs for Aβ deposition across CN, MCI, and AD groups. In the All group (CN+MCI+AD) and CN group, only the inferior orbital frontal cortex (IOFC) showed modest associations. AD exhibited predictive BM hubs in the Rolandic operculum (RO) and precentral gyrus (PreCG), while MCI demonstrated the highest sensitivity with hubs in the superior/middle temporal gyri (STG/MTG), middle cingulate (MCC), precuneus (PCUN), and Heschl's gyrus; (b) Inverse correlation between aggregated BM values of top-predictive hubs and global Aβ burden (SUVR). The strongest association was observed in MCI, indicating BM's neuroprotective role against amyloid accumulation during preclinical stages. Pearson correlation tests were two-sided, and P values were corrected for multiple comparisons. Exact P values are shown in the panel where possible.
Note: The statistical results are reported at the group level: predictive regions were identified using LOOCV (panel a), and BM values from these hubs were then extracted across all participants to evaluate associations with global Aβ deposition. Panel a was generated using Python. Panel b was generated using MATLAB (MathWorks, Natick, MA, USA).

Editor's Summary: Using multimodal MRI and PET across healthy and pathological aging, the authors derive a structure-function brain maintenance metric that predicts cognitive resilience, slower decline, and lower amyloid burden.

Peer review information: *Nature Communications* thanks Lars Nyberg who co-reviewed with Emma Rodrigues; and the other, anonymous, reviewer(s) for their contribution to the peer review of this work. A peer review file is available.

a

Sub.1
Sub.2
Sub.3
…
Sub.n

T1-weighted

Surface restructuration

Sub.1
Sub.2
Sub.3
…
Sub.n

Individual's native space

Resample & smooth

Sub.1
Sub.2
Sub.3
…
Sub.n

fsaverage space

Thickness of each Vertex

Sub.1 Sub.2 Sub.3 Sub.4 Sub.5 Sub.6 Sub.7 Sub.8 Sub.9 Sub.10 Sub. n

Vertex X TR

Sub.1 Sub.2 Sub.n

b

Feature Vectors

Reconstruction

Empirical

Frobenius norm

$$|A|_F = \sqrt{\sum_{i=1}^{m}\sum_{j=1}^{n}|a_{ij}|^2}$$

Vertex FC matrix in each parcel

Schaefer2018 400 parcel parcellation

input

Thickness of older individuals

model

Reconstruction

Functional timeseries

Time

Rejuvenation-Oriented Structural-Functional Brain Prediction Model

Generate model parameters

1 2 3 4 … n

LOO-CV

Model Training

c

①

$N_{(subjects)} \times P_{(parcels)}$

Correlation maximization

$N_{(subjects)} \times Q_{(tests)}$

MMSE
AVLT-N1N5
SDMT
TMT-A
SCWT C-B
TMT-B
CDT
CVFT
CDT

Longitudinal Data

②

Calculation of Cognitive Aging Rate

T2

T1

Parcels

Sub.N

10-fold CV

GLM

MMSE SDMT AVLT TMT-A

Cognitive Aging Rate

CR Scores

Disease Cohort

③

$Y = B_0 + B_1 * X$

X: Neighborhood matrix of parcels of ODD-CR regions

Y: Aβ accumulation of each individual's whole brain

CR values

Aβ accumulation

RMSE

ALL Groups MCI Group CN Group AD Group

Parcel 1
Parcel 2
Parcel 3
Parcel 4
Parcel 5
Parcel 6

CR Weight

BM Scores

Cognitive Scores

BM Scores

SCCA Analysis

Parcel 1
Parcel 2
Parcel 3
Parcel 4
Parcel 5
Parcel 6

Cognitive Weight

Cognitive Scores

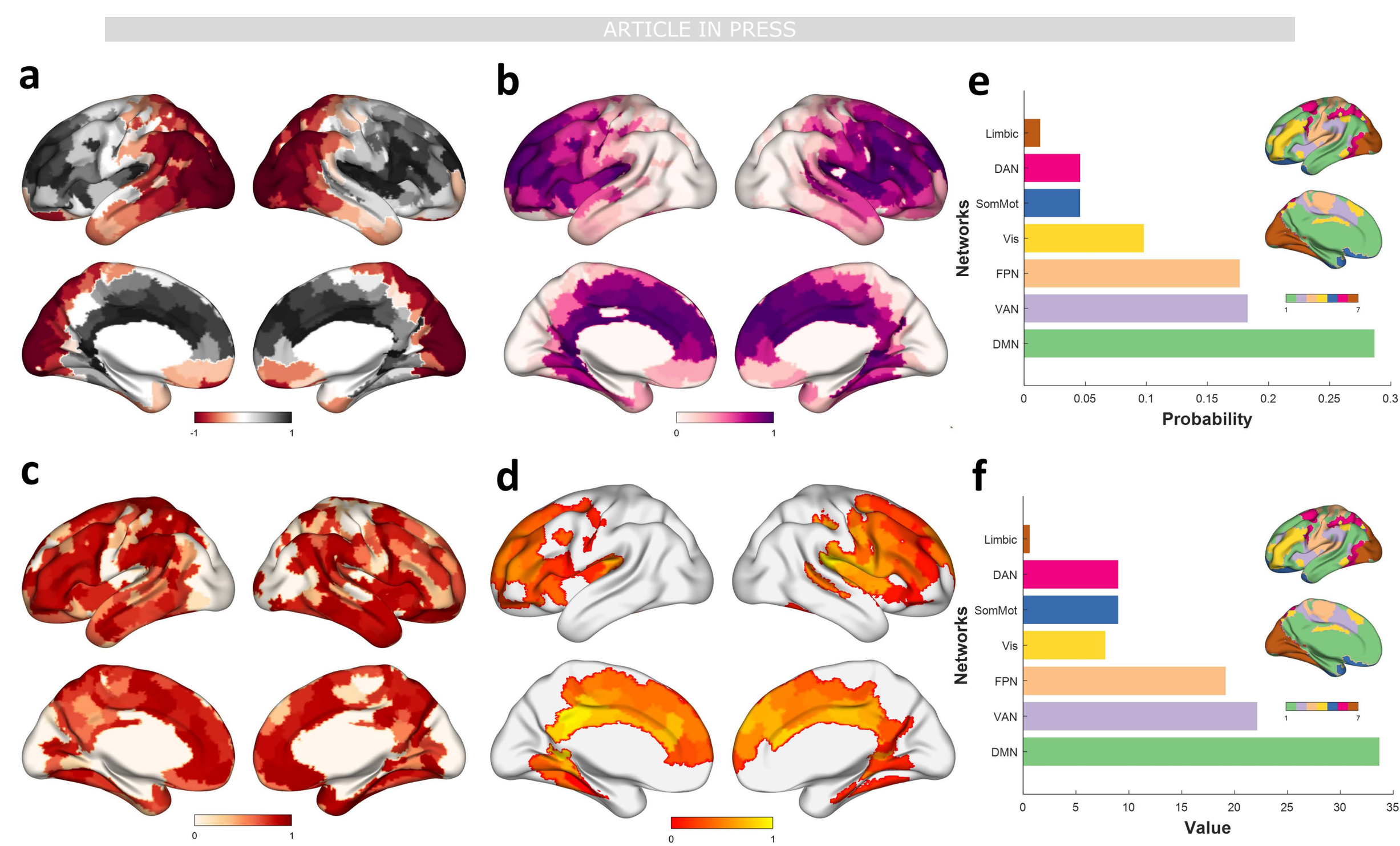
a
-1
1
b
0
1
e
Limbic
DAN
SomMot
Vis
FPN
VAN
DMN
Networks
0
0.05
0.1
0.15
0.2
0.25
0.3
Probability
1
7
c
0
1
d
0
1
f
Limbic
DAN
SomMot
Vis
FPN
VAN
DMN
Networks
0
5
10
15
20
25
30
35
Value
1
7

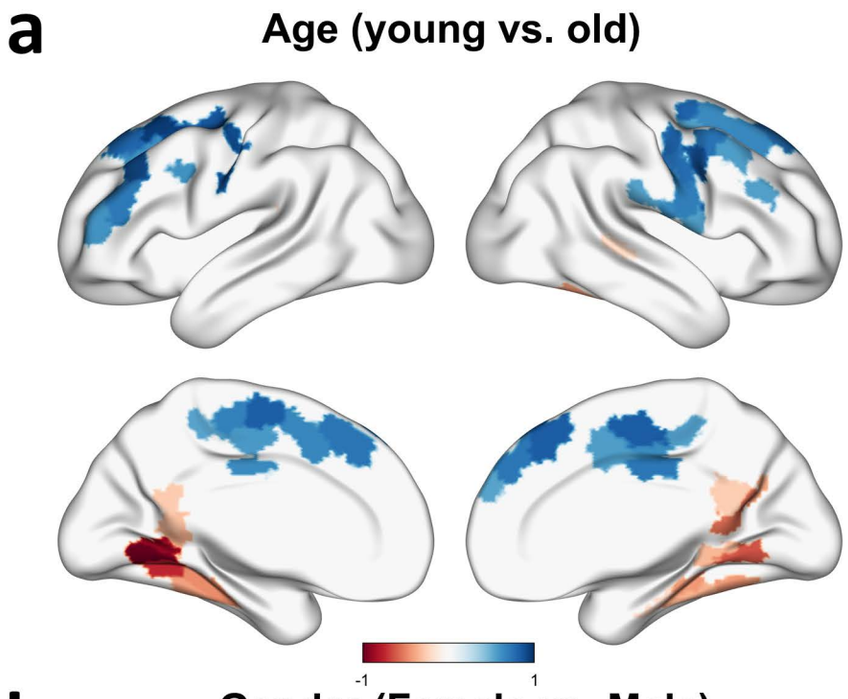
a
Age (young vs. old)
-1
1

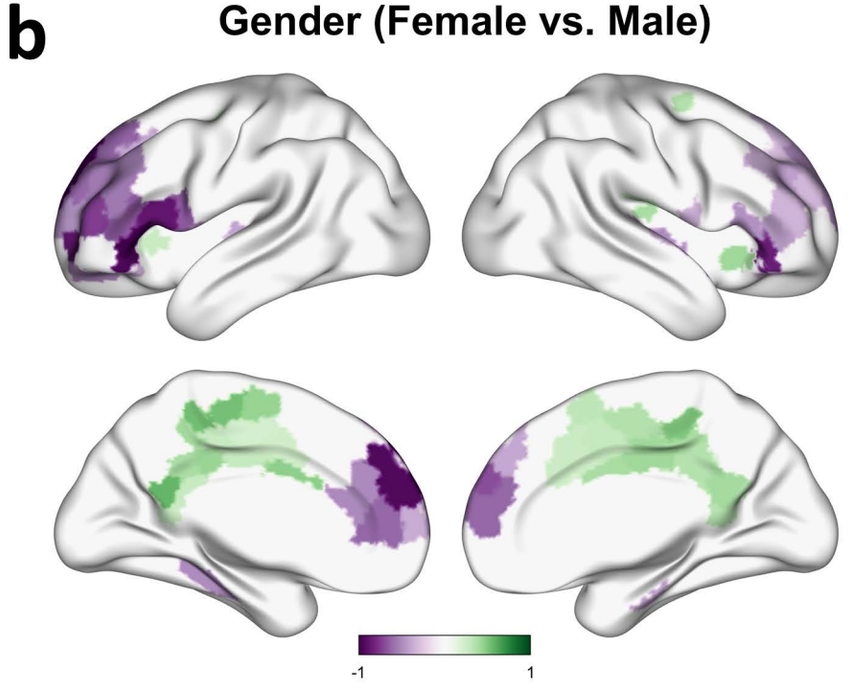
b
Gender (Female vs. Male)
-1
1

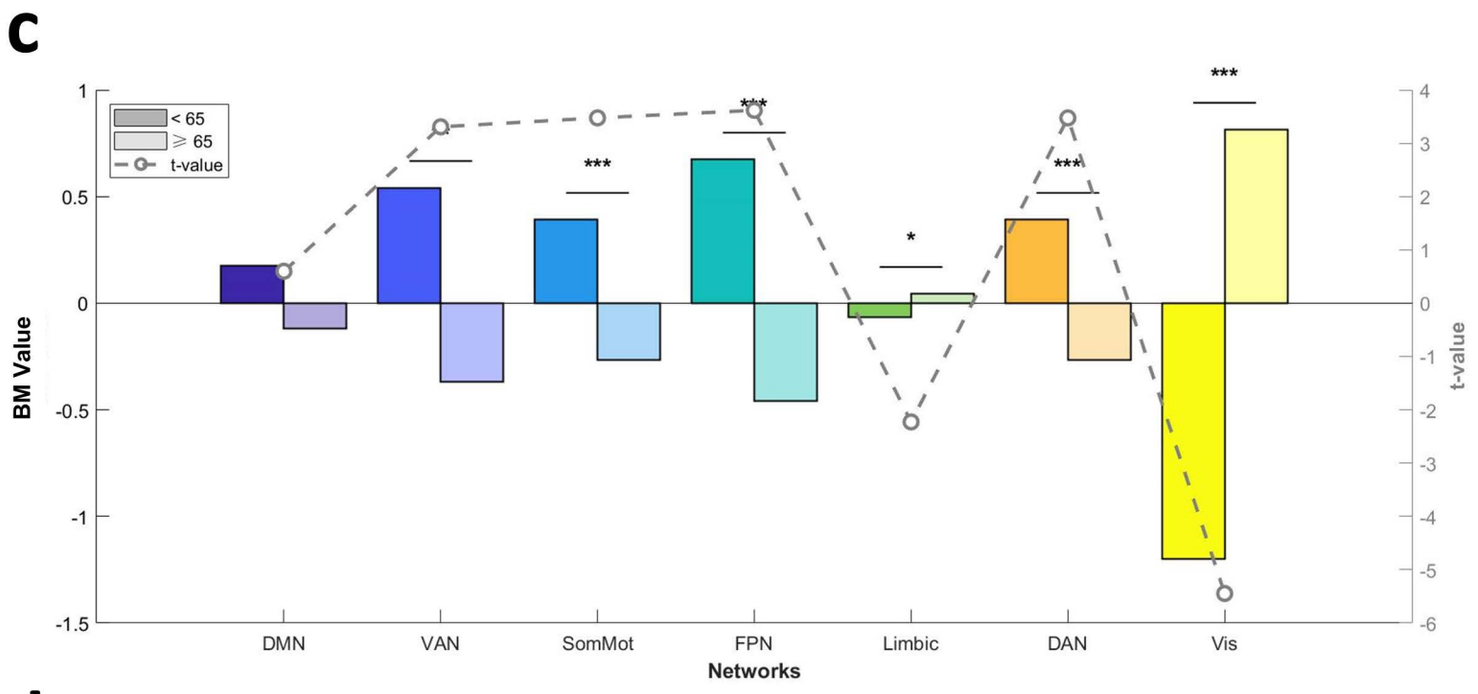
c
< 65
⩾ 65
t-value
BM Value
t-value
DMN
VAN
SomMot
FPN
Limbic
DAN
Vis
Networks

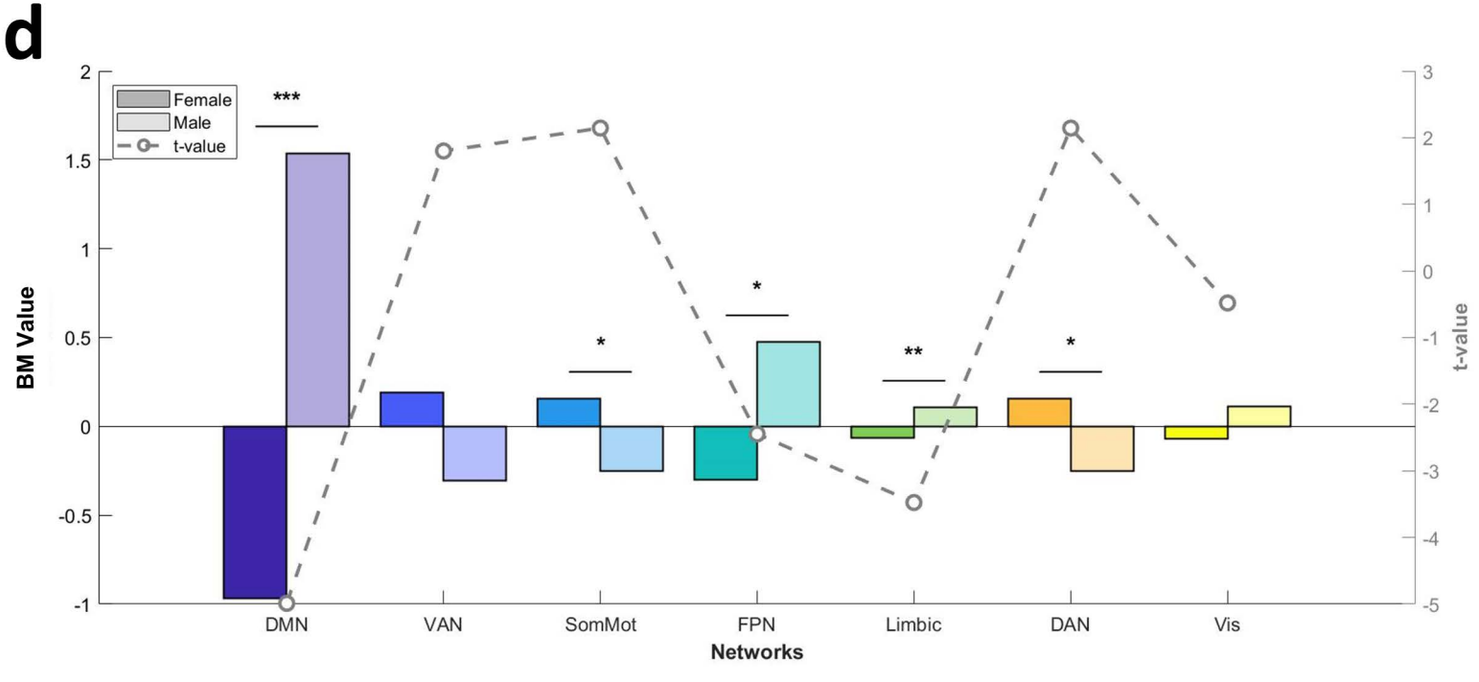
d
Female
Male
t-value
BM Value
t-value
DMN
VAN
SomMot
FPN
Limbic
DAN
Vis
Networks

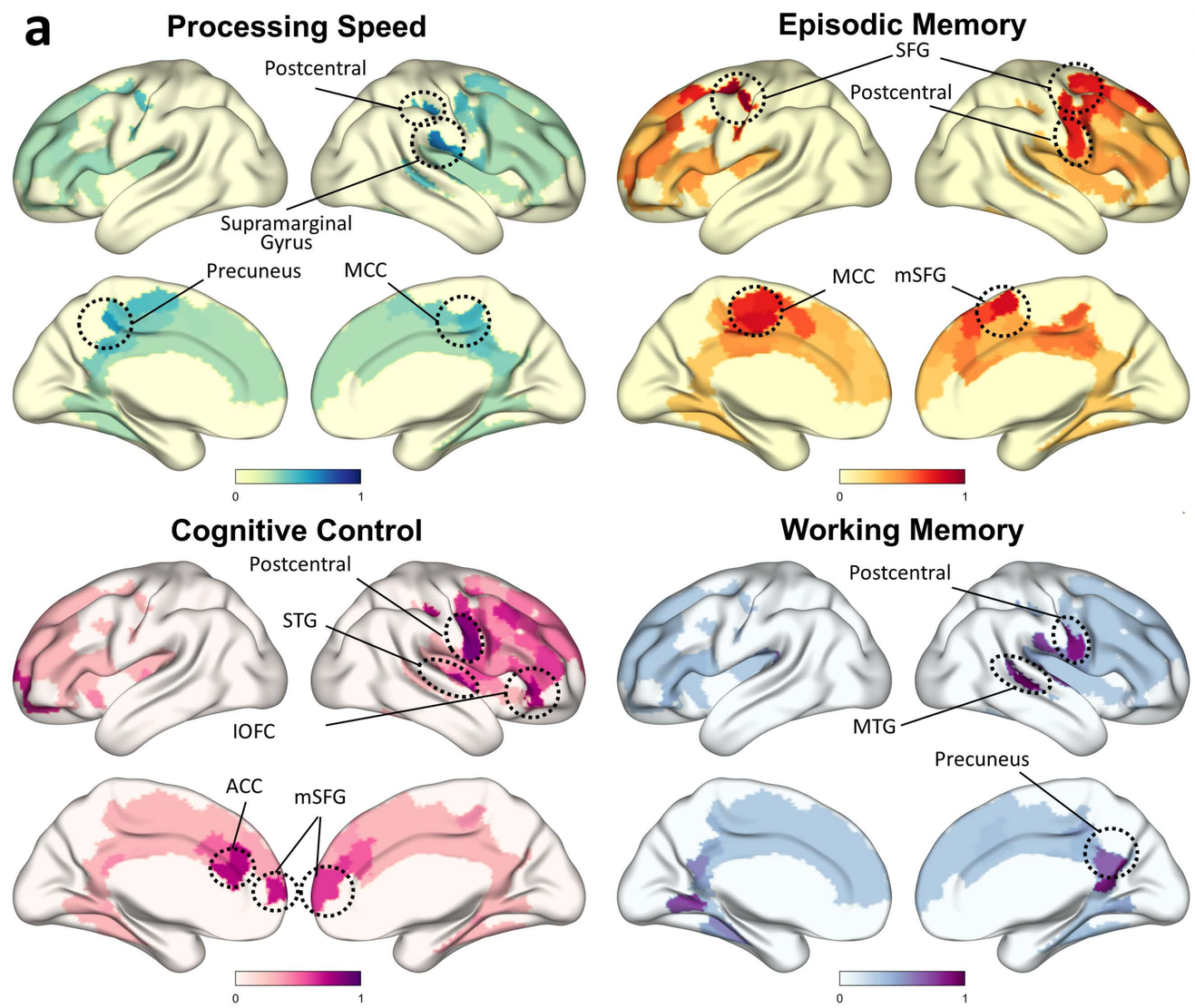
a
Processing Speed
Postcentral
Supramarginal Gyrus
Precuneus
MCC
0
1
Episodic Memory
SFG
Postcentral
MCC
mSFG
0
1
Cognitive Control
Postcentral
STG
IOFC
ACC
mSFG
0
1
Working Memory
Postcentral
MTG
Precuneus
0
1

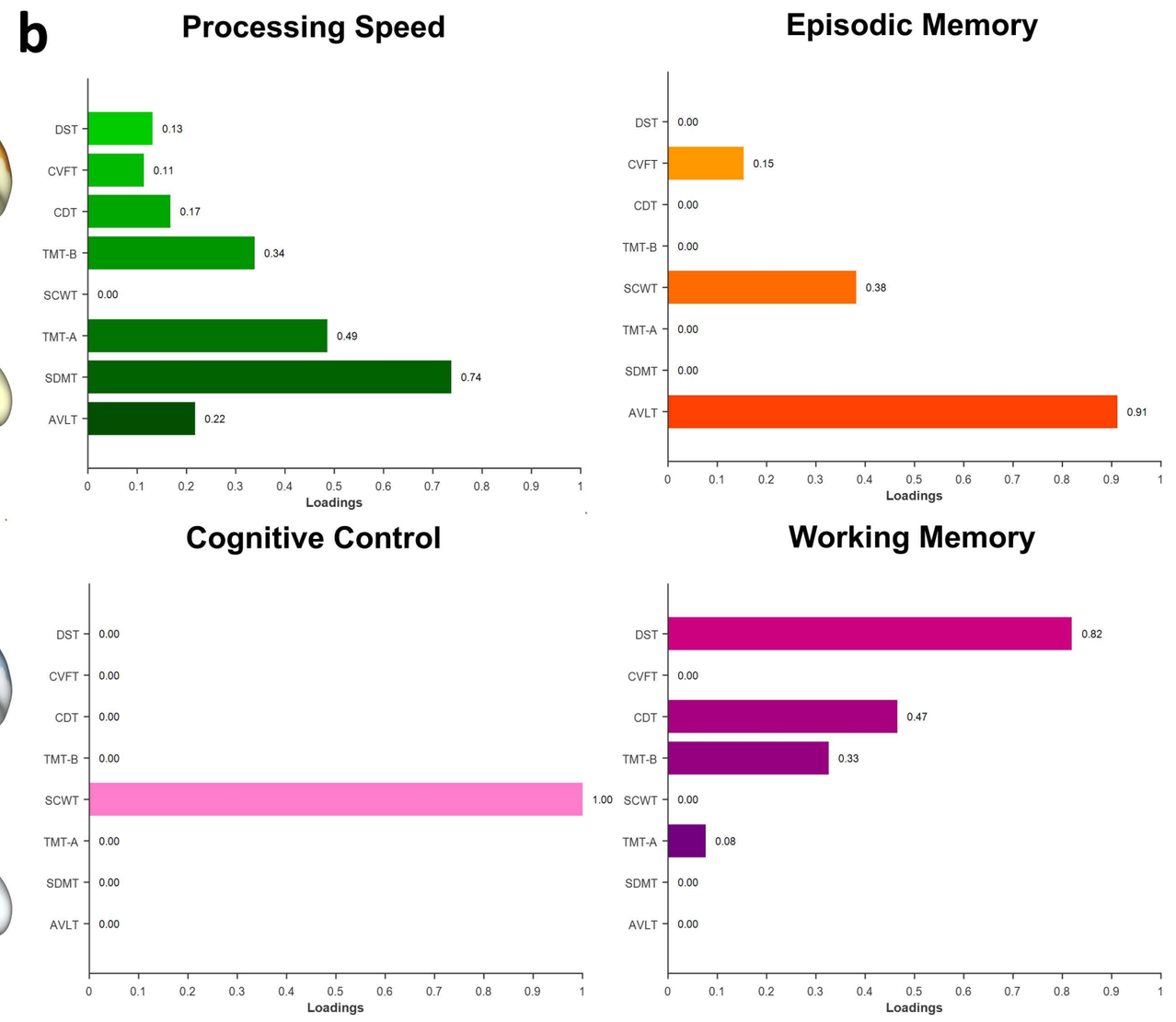
b
Processing Speed
DST 0.13
CVFT 0.11
CDT 0.17
TMT-B 0.34
SCWT 0.00
TMT-A 0.49
SDMT 0.74
AVLT 0.22
Loadings
Episodic Memory
DST 0.00
CVFT 0.15
CDT 0.00
TMT-B 0.00
SCWT 0.38
TMT-A 0.00
SDMT 0.00
AVLT 0.91
Loadings
Cognitive Control
DST 0.00
CVFT 0.00
CDT 0.00
TMT-B 0.00
SCWT 1.00
TMT-A 0.00
SDMT 0.00
AVLT 0.00
Loadings
Working Memory
DST 0.82
CVFT 0.00
CDT 0.47
TMT-B 0.33
SCWT 0.00
TMT-A 0.08
SDMT 0.00
AVLT 0.00
Loadings


c
R Processing Spped = 0.10 , P < 0.001
Processing Speed
BM Value
Processing Speed (Bottom: Light → Top: Dark)
R Episodic Memory = 0.12 , P < 0.001
Episodic Memory
BM Value
Episodic Memory (Bottom: Light → Top: Dark)
R Cognitive Control = 0.08 , P = 0.003
Cognitive Control
BM Value
Cognitive Control (Bottom: Light → Top: Dark)
R Working Memory = 0.11 , P < 0.001
Working Memory
BM Value
Working Memory (Bottom: Light → Top: Dark)

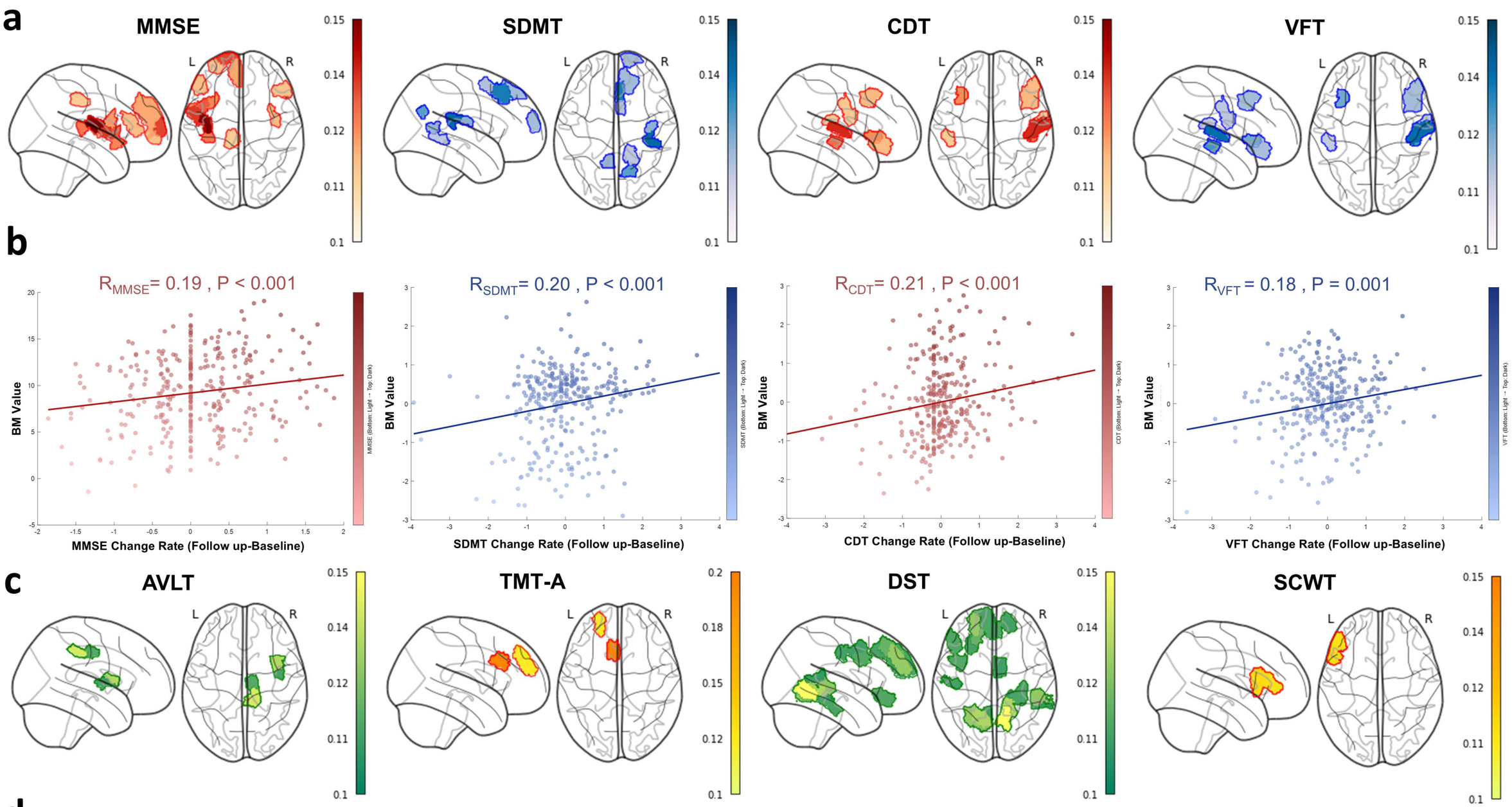
a
MMSE
SDMT
CDT
VFT
L
R
0.15
0.14
0.12
0.11
0.1
b
R_{MMSE}= 0.19 , P < 0.001
R_{SDMT}= 0.20 , P < 0.001
R_{CDT}= 0.21 , P < 0.001
R_{VFT} = 0.18 , P = 0.001
BM Value
MMSE (Bottom: Light → Top: Dark)
SDMT (Bottom: Light → Top: Dark)
CDT (Bottom: Light → Top: Dark)
VFT (Bottom: Light → Top: Dark)
MMSE Change Rate (Follow up-Baseline)
SDMT Change Rate (Follow up-Baseline)
CDT Change Rate (Follow up-Baseline)
VFT Change Rate (Follow up-Baseline)
c
AVLT
TMT-A
DST
SCWT
0.2
0.18
0.15
d
R_{AVLT}= 0.18 , P = 0.001
R_{TMT-A} = 0.26 , P < 0.001
R_{DST}= 0.19 , P < 0.001
R_{SCWT} = 0.18 , P = 0.03
AVLT (Bottom: Light → Top: Dark)
TMT-A (Bottom: Light → Top: Dark)
DST (Bottom: Light → Top: Dark)
SCWT C-B (Bottom: Light → Top: Dark)
AVLT Change Rate (Follow up-Baseline)
TMT-A Change Rate (Follow up-Baseline)
DST Change Rate (Follow up-Baseline)
SCWT Change Rate (Follow up-Baseline)

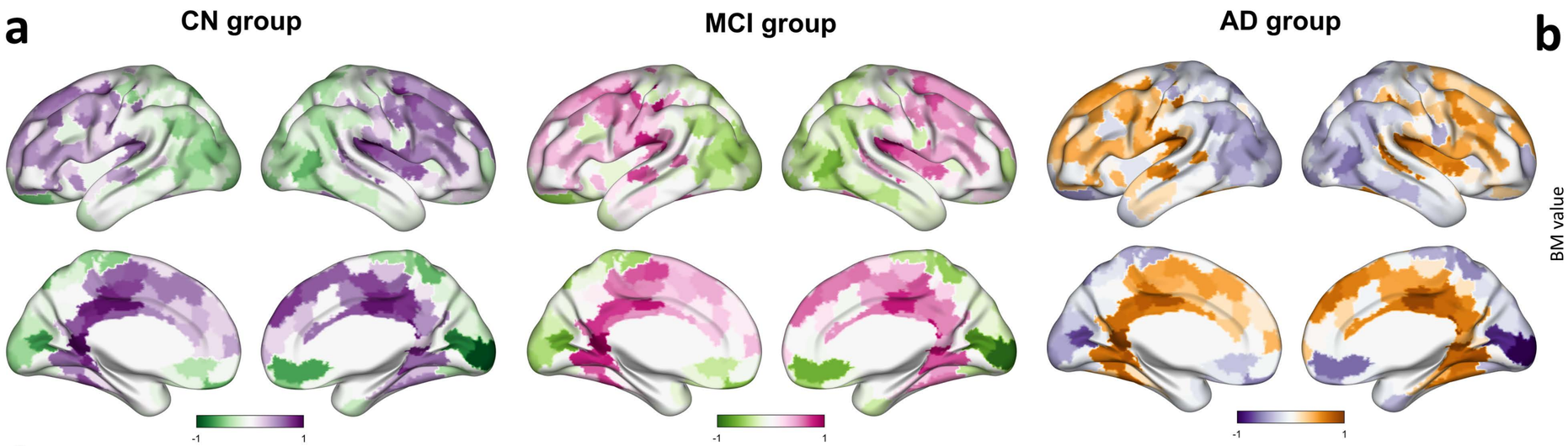
a
CN group
MCI group
AD group
-1
1

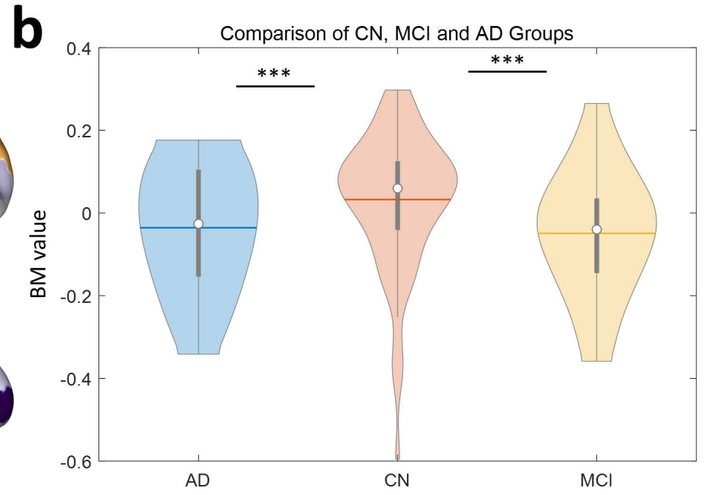
b
Comparison of CN, MCI and AD Groups
***
***
BM value
AD
CN
MCI

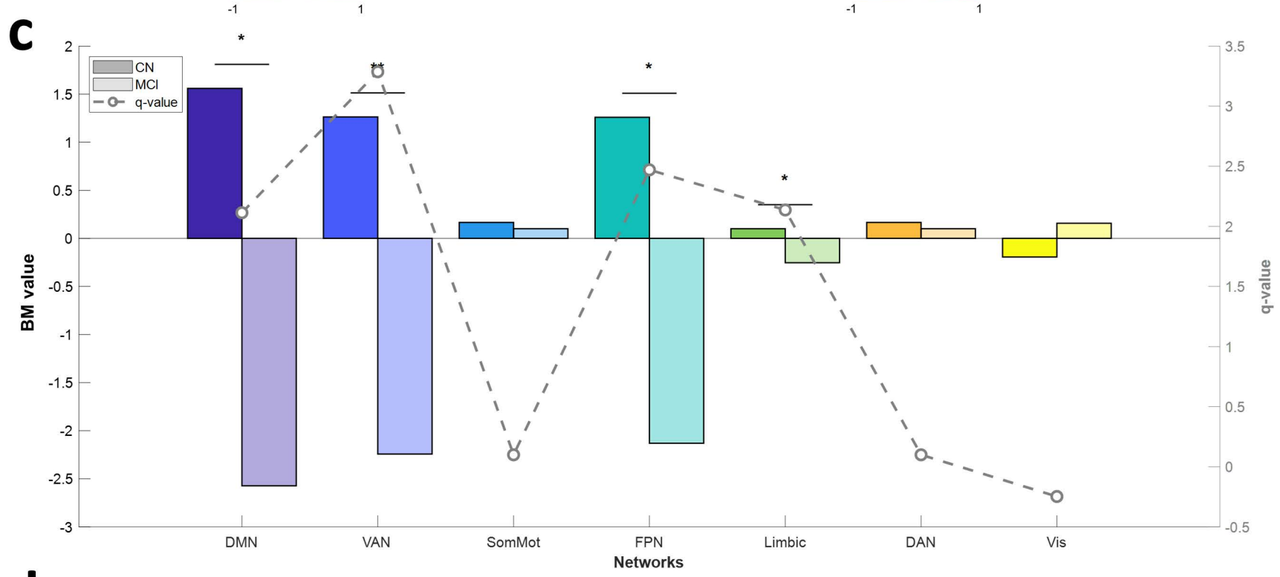
c
CN
MCI
q-value
BM value
q-value
DMN
VAN
SomMot
FPN
Limbic
DAN
Vis
Networks

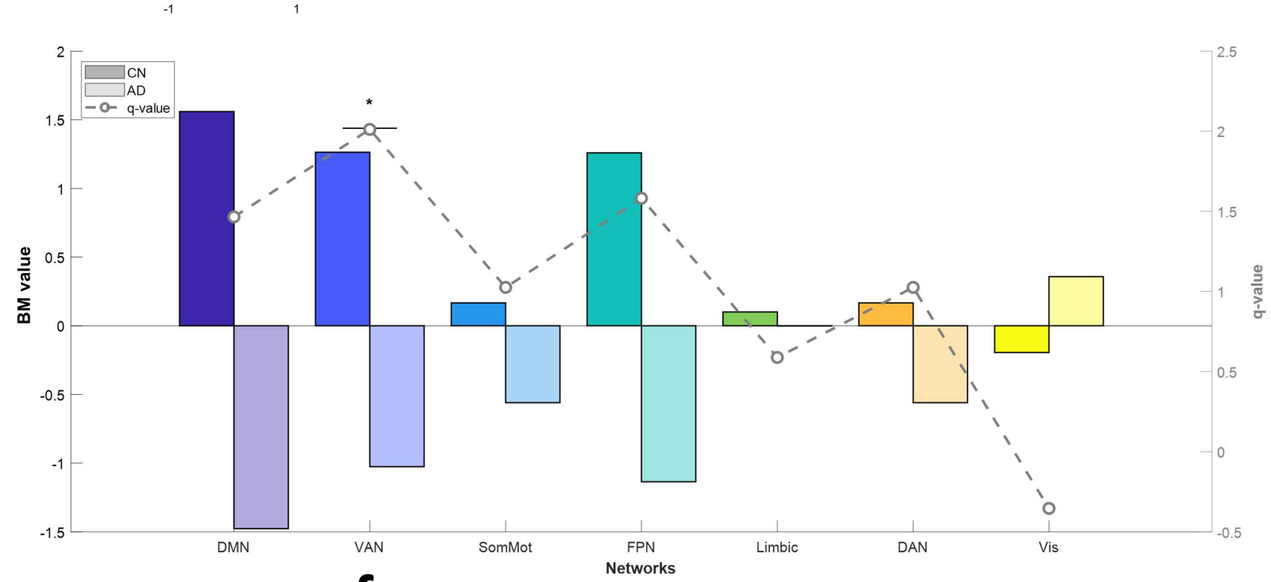
CN
AD
q-value
BM value
q-value
DMN
VAN
SomMot
FPN
Limbic
DAN
Vis
Networks

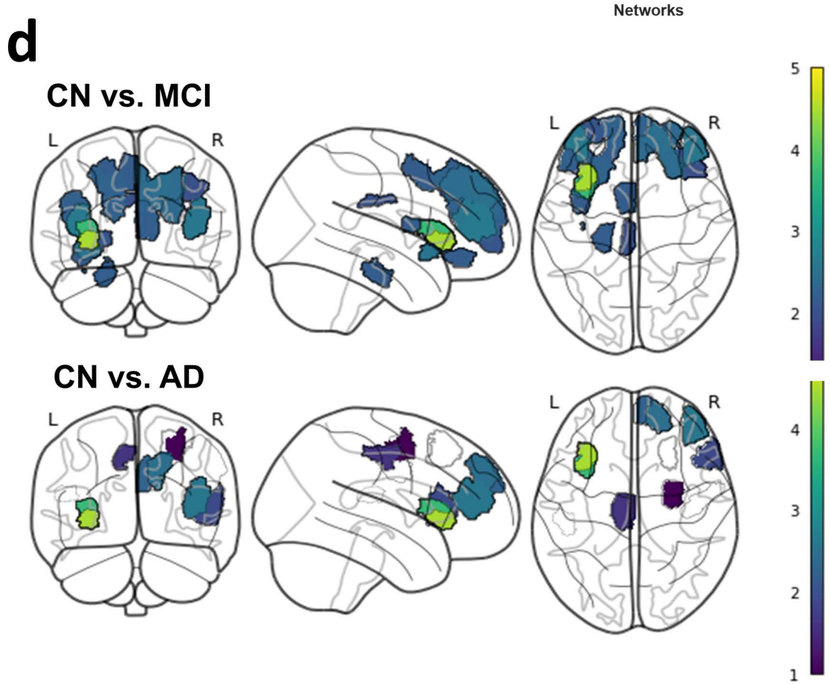
d
CN vs. MCI
CN vs. AD
L
R

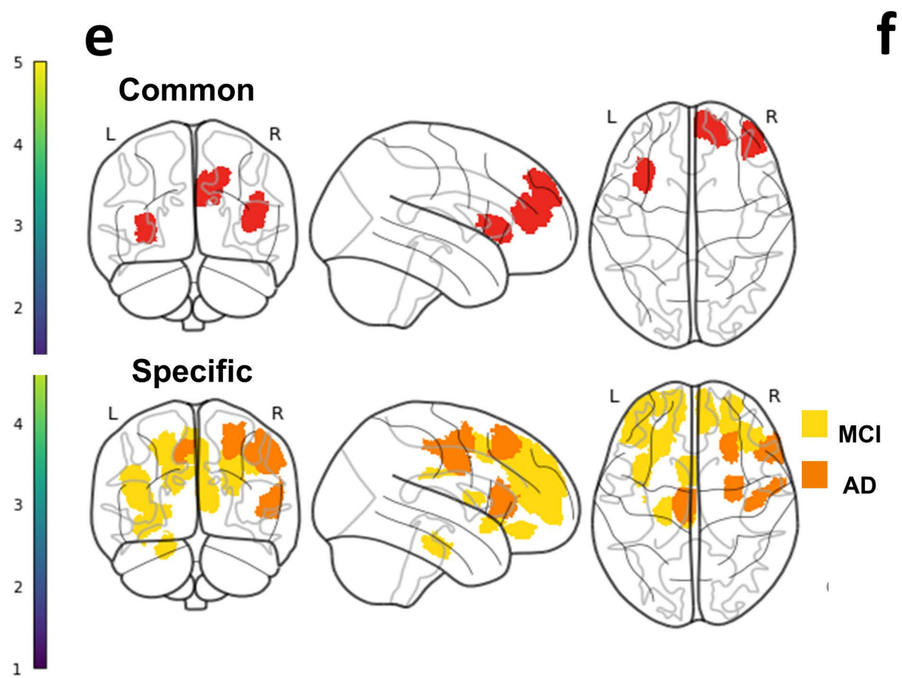
e
Common
Specific
L
R
MCI
AD

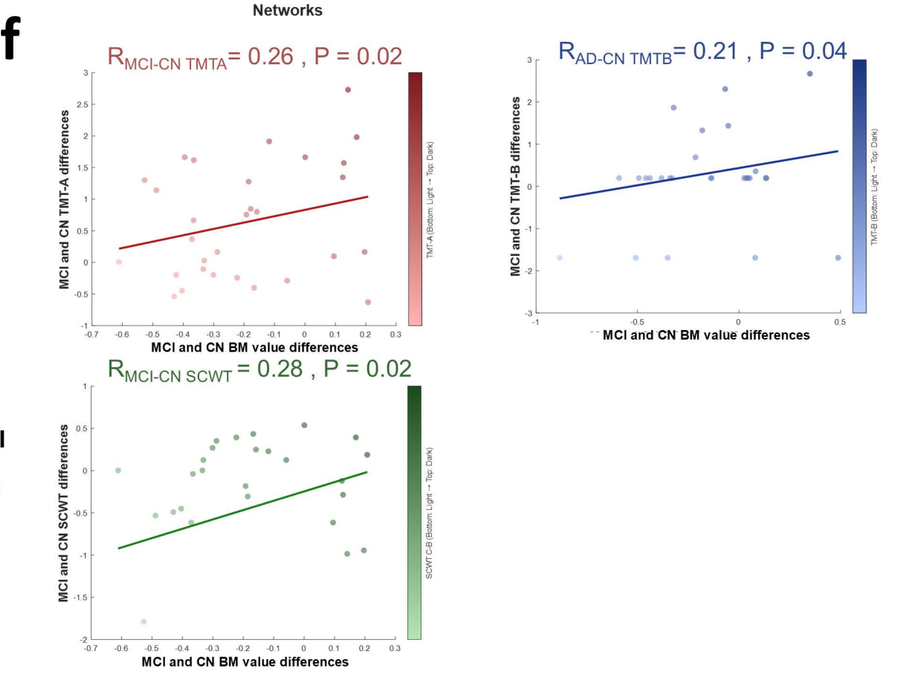
f
R MCI-CN TMTA = 0.26 , P = 0.02
MCI and CN TMT-A differences
MCI and CN BM value differences
R AD-CN TMTB = 0.21 , P = 0.04
MCI and CN TMT-B differences
MCI and CN BM value differences
R MCI-CN SCWT = 0.28 , P = 0.02
MCI and CN SCWT differences
MCI and CN BM value differences

a

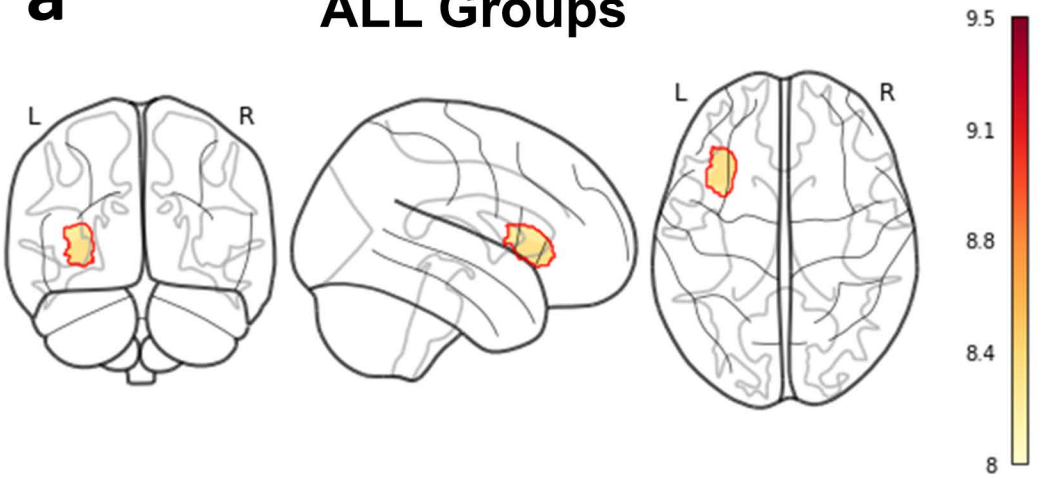
ALL Groups
L
R
9.5
9.1
8.8
8.4
8

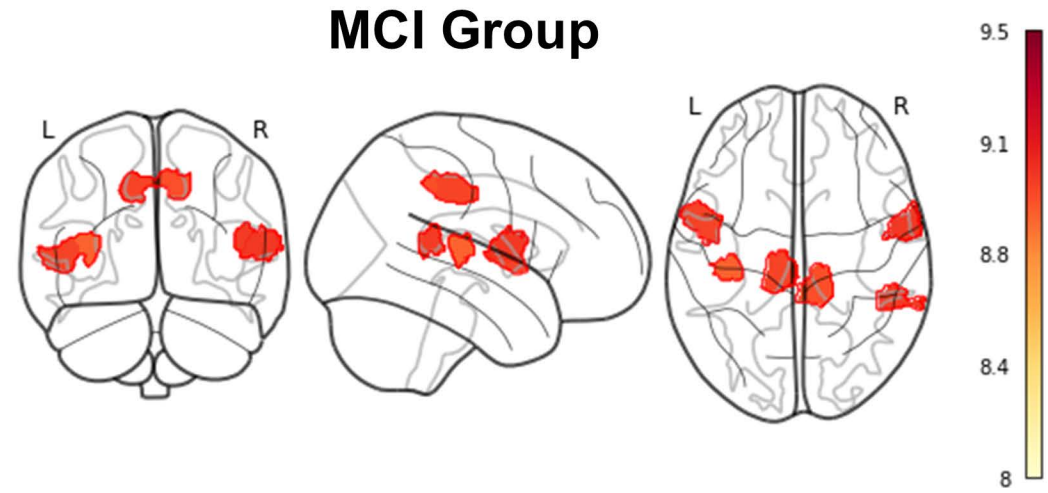
MCI Group
L
R
9.5
9.1
8.8
8.4
8

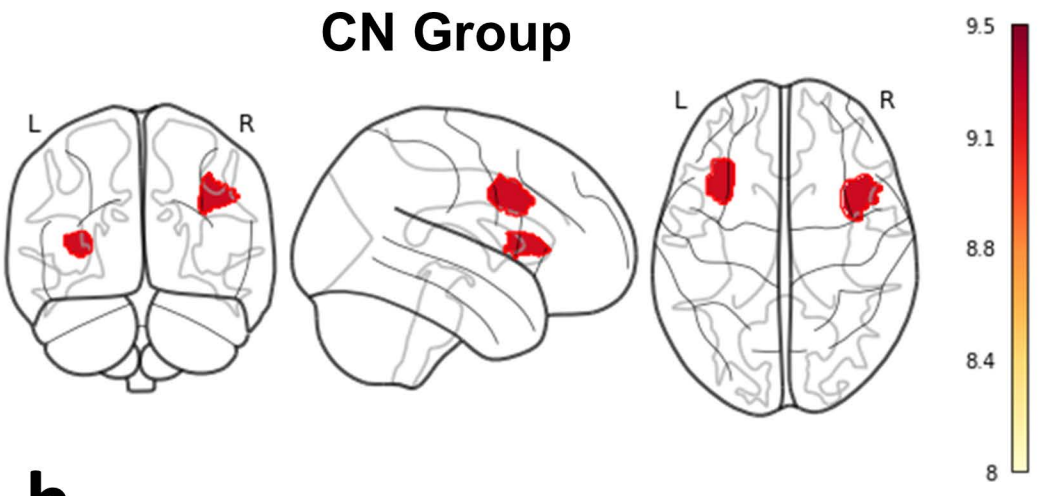
CN Group
L
R
9.5
9.1
8.8
8.4
8

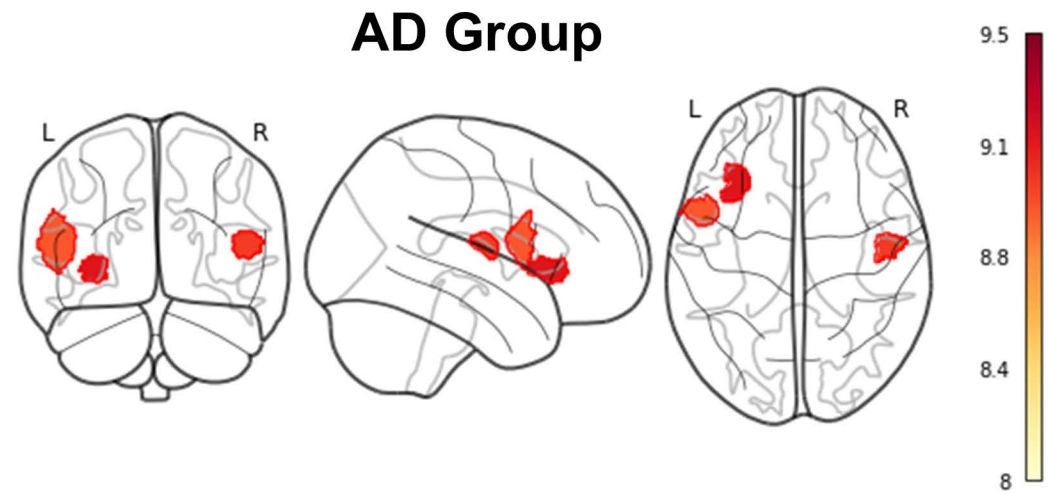
AD Group
L
R
9.5
9.1
8.8
8.4
8

b

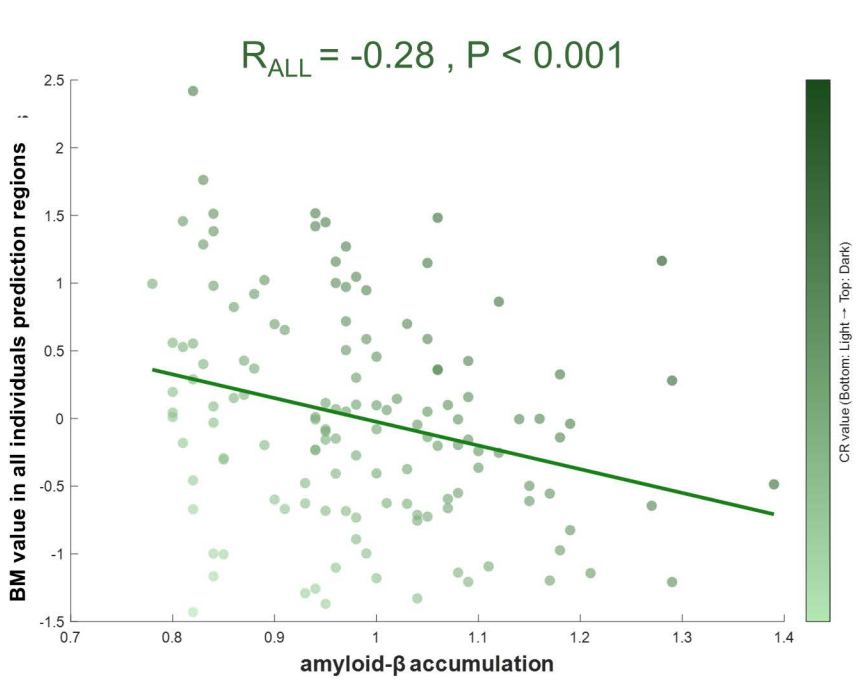
R_ALL = -0.28 , P < 0.001
BM value in all individuals prediction regions
amyloid-β accumulation
CR value (Bottom: Light → Top: Dark)

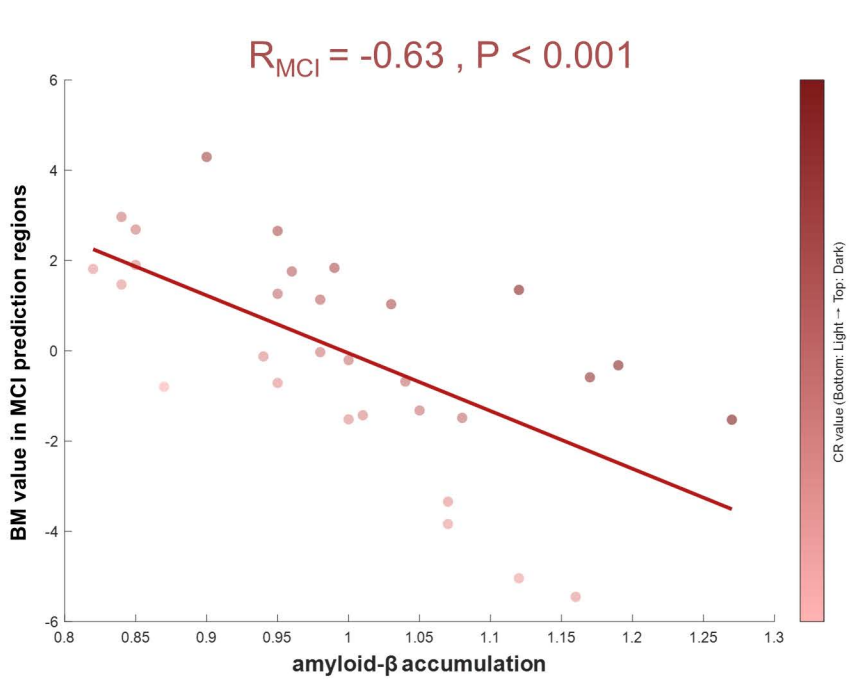
R_MCI = -0.63 , P < 0.001
BM value in MCI prediction regions
amyloid-β accumulation
CR value (Bottom: Light → Top: Dark)

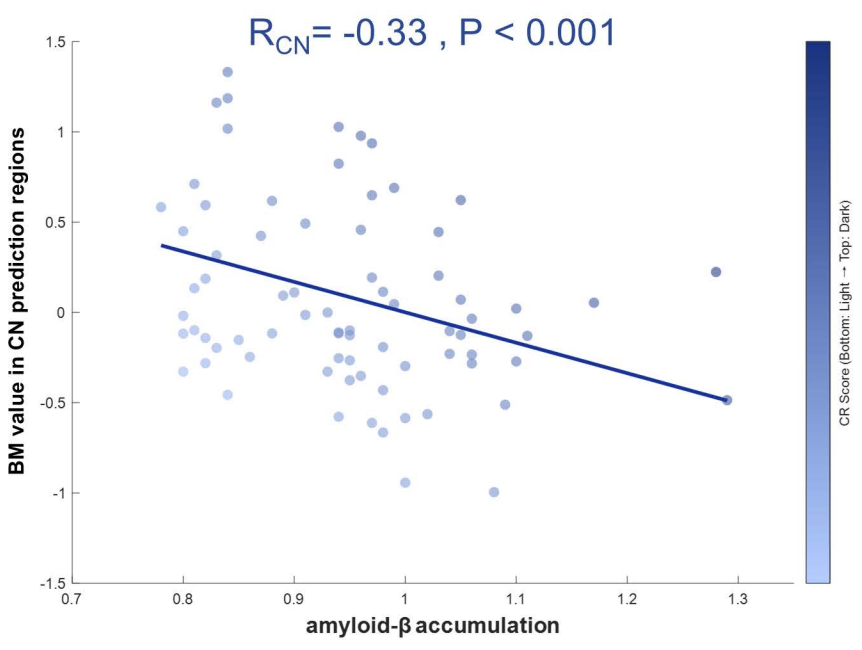
R_CN= -0.33 , P < 0.001
BM value in CN prediction regions
amyloid-β accumulation
CR Score (Bottom: Light → Top: Dark)

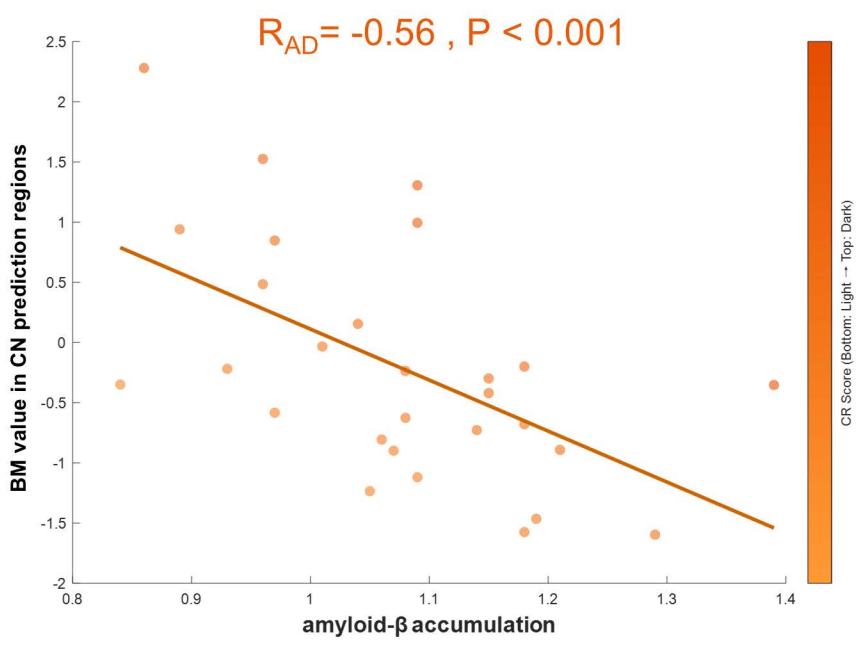
R_AD= -0.56 , P < 0.001
BM value in CN prediction regions
amyloid-β accumulation
CR Score (Bottom: Light → Top: Dark)